

Explosive neural networks via higher-order interactions in curved statistical manifolds

Miguel Aguilera*

*BCAM – Basque Center for Applied Mathematics, Bilbao, Spain
IKERBASQUE, Basque Foundation for Science, Bilbao, Spain*

Pablo A. Morales

*Research Division, Araya Inc., Tokyo, Japan
Centre for Complexity Science, Imperial College London, London, UK*

Fernando E. Rosas

*Department of Informatics, University of Sussex, Brighton, UK
Sussex Centre for Consciousness Science and Sussex AI, University of Sussex, Brighton, UK
Department of Brain Science, Imperial College London, London, UK
Center for Eudaimonia and Human Flourishing, University of Oxford, Oxford, UK*

Hideaki Shimazaki

*Graduate School of Informatics, Kyoto University, Kyoto, Japan
Center for Human Nature, Artificial Intelligence,
and Neuroscience (CHAIN), Hokkaido University, Sapporo, Japan*

Higher-order interactions underlie complex phenomena in systems such as biological and artificial neural networks, but their study is challenging due to the scarcity of tractable models. By leveraging a generalisation of the maximum entropy principle, here we introduce *curved neural networks* as a class of prototypical models with a limited number of parameters that are particularly well-suited for studying higher-order phenomena. Through exact mean-field descriptions, we show that these curved neural networks implement a self-regulating annealing process that can accelerate memory retrieval, leading to explosive order-disorder phase transitions with multi-stability and hysteresis effects. Moreover, by analytically exploring their memory-retrieval capacity using the replica trick near ferromagnetic and spin-glass phase boundaries, we demonstrate that these networks can enhance memory capacity and robustness of retrieval over classical associative-memory networks. Overall, the proposed framework provides parsimonious models amenable to analytical study, revealing novel higher-order phenomena in complex networks.

INTRODUCTION

Complex physical, biological, and social systems often exhibit higher-order interdependencies that cannot be reduced to pairwise interactions between their components [1, 2]. Recent studies suggest that higher-order organisation is not the exception but the norm, providing various mechanisms for its emergence [3–6]. Modelling studies have revealed that higher-order interactions (HOIs) underlie collective activities such as bistability, hysteresis, and ‘explosive’ phase transitions associated with abrupt discontinuities in order parameters [4, 7–11].

HOIs are particularly important for the functioning of biological and artificial neural systems. For instance, they shape the collective activity of biological neurons [12, 13], being directly responsible for their inherent sparsity [5, 13–15] and possibly underlying critical dynamics [16, 17]. HOIs have also been shown to enhance the computational capacity of artificial recurrent neural networks [18, 19]. More specifically, ‘dense associative memories’ with extended memory capacity [20–23] are realised

by specific non-linear activation functions, which effectively incorporate HOIs. These non-linear functions are related to attention mechanisms of transformer neural networks [24] and the energy landscape of diffusion models [25, 26], leading to conjecture that HOIs underlie the success of these state-of-the-art deep learning models.

Despite their importance, existent studies of HOIs face significant computational challenges. Analytically tractable models that incorporate HOIs typically limit interactions to a single order (e.g., p-spin models [22, 27, 28]). Otherwise, attempting to represent diverse HOIs exhaustively results in a combinatorial explosion [29]. This issue is pervasive, restricting investigations of high-order interaction models — such as contagion [9], Ising [19] or Kuramoto [30] models — to highly homogeneous scenarios [3, 16] or to models of relatively low-order [9, 11, 31]. While attempts have been made to model all orders of HOIs and perform theoretical analyses [20–23, 32–37], it is currently unclear how to construct parsimonious models to address the diverse effects of HOIs in a principled manner.

To address this challenge, here we employ an extension of the maximum entropy principle to capture HOIs through the deformation of the space of statistical models. When applied to neural networks, our approach gen-

* maguilera@bcamath.org

eralises classical neural network models to yield a family of *curved neural networks*, which effectively incorporate all orders of HOIs even if the model’s statistics are restricted to low-order. The resulting models have rich connections with the literature on the statistical physics of neural networks [21, 22, 27, 34]. These features enable the exploration of various aspects of HOIs using techniques including mean-field approximations, quenched disorder analyses, and path integrals.

Our analyses reveal how relatively simple curved neural networks exhibit some of the hallmark characteristics of higher-order phenomena, such as explosive phase transitions, arising both in mean-field models and in more complex transitions to spin-glass states. These phenomena are driven by a self-regulated annealing process, which accelerates memory retrieval through positive feedback between energy and an ‘effective’ temperature. Furthermore, we show — both analytically and experimentally — that this mechanism can lead to an increase in the memory capacity or robustness of memory retrieval in these neural networks. Overall, the core contributions of this work are (i) the development of a parsimonious neural network model based on the maximum entropy principle that captures interactions of all orders, (ii) the discovery of a self-regulated annealing mechanism that can drive explosive phase transitions, and (iii) the demonstration of enhanced memory capacity resulting from this mechanism.

RESULTS

High-order interactions in curved manifolds

Generalised maximum entropy principle

The maximum entropy principle (MEP) is a general modelling framework based on the principle of adopting the model with maximal entropy compatible with a given set of observations, under the rationale that one should not include structure that is not in the assumptions or the selected features of data [38, 39]. The traditional formulation of the MEP is based on Shannon’s entropy [40], and the resulting models correspond to Boltzmann distributions of the form $p(\mathbf{x}) = \exp(\sum_a \theta_a f_a(\mathbf{x}) - \varphi)$, where φ is a normalising potential and θ_a are parameters constraining the average value of observables $\langle f_a(\mathbf{x}) \rangle$. While observables are often set to low orders (e.g. $f_i(\mathbf{x}) = x_i$, $f_{i,j}(\mathbf{x}) = x_i x_j$, corresponding to first and second order statistics), higher-order interdependencies can be included by considering observables of the type $f_I(\mathbf{x}) = \prod_{i \in I} x_i$, where I is a set of indices of order $k = |I|$. Unfortunately, an exhaustive description of interactions up to order $k \gg 1$ becomes unfeasible in practice due to an exponential number of terms (for more details on the MEP, see Supplementary Note 1).

The MEP can be expanded to include other entropy functionals such as Tsallis’ [41] and Rényi’s [42]. Con-

cretely, maximising the Rényi entropy (with the scaling parameter $\gamma \geq -1$) [43]

$$H_\gamma(p) = -\frac{1}{\gamma} \log \sum_{\mathbf{x}} p(\mathbf{x})^{1+\gamma} \quad (1)$$

while constraining $\langle f_a(\mathbf{x}) \rangle$ (i.e., the expectation of features by $p(\mathbf{x})$) results in models of the form (see Supplementary Note 1):

$$p_\gamma(\mathbf{x}) = \exp(-\varphi_\gamma) \left[1 + \gamma\beta \sum_a \theta_a f_a(\mathbf{x}) \right]_+^{1/\gamma}, \quad (2)$$

where φ_γ is a normalising constant given by

$$\varphi_\gamma = \log \sum_{\mathbf{x}} \left[1 + \gamma\beta \sum_a \theta_a f_a(\mathbf{x}) \right]_+^{1/\gamma}. \quad (3)$$

Above, the square bracket operator sets negative values to zero, $[x]_+ = \max\{0, x\}$. We refer to distributions following (2) as the *deformed exponential family* distributions, which maximises both Rényi and Tsallis entropies [44]. When $\gamma \rightarrow 0$, Rényi’s entropy tends to Shannon’s and (2) to the standard exponential family [42].

A fundamental insight explored in this paper is that higher-order interdependencies can be efficiently captured by deformed exponential family distributions [45, 46]. Starting from a standard Shannon’s MEP model with low-order interactions, it can be shown that varying γ in (2) results in a deformation of the statistical manifold which, in turn, enhances the capability of $p_\gamma(\mathbf{x})$ to account for higher-order interdependencies. In effect, the consequence of deformation can be investigated by rewriting (2) via Taylor expansion of the exponent

$$p_\gamma(\mathbf{x}) = \exp \left(\sum_{k=1}^{\infty} \frac{-1}{k\gamma} \left(-\gamma\beta \sum_a \theta_a f_a(\mathbf{x}) \right)^k - \varphi_\gamma \right), \quad (4)$$

which is valid for the case $1 + \gamma \sum_a \theta_a f_a(\mathbf{x}) > 0$, and otherwise $p_\gamma(\mathbf{x}) = 0$. This shows that the deformed manifold contains interactions of all orders even if $f_a(\mathbf{x})$ is restricted to lower orders while establishing a specific dependency structure across the orders, thereby avoiding a combinatorial explosion of the number of required parameters. The deformation resulting from the maximisation of a non-Shannon entropy has been shown to reflect a curvature of the space of possible models in information geometry [42, 47]. This leads to a particular *foliation* of the space of possible models [48] (an ‘onion-like’ manifold structure, Fig. 1), which has properties that allow to re-derive the MEP from fundamental geometric properties — for technical details, see Supplementary Note 1.

Curved neural networks

Several well-known neural network models adhere to the MEP, such as Ising-like models [49] and Boltzmann

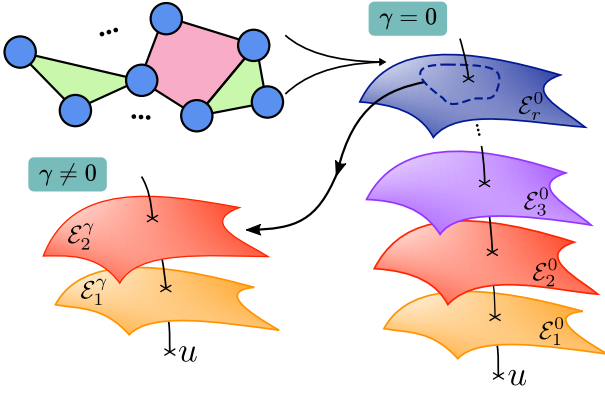


FIG. 1. **Higher-order decomposition resulting from the foliation of a statistical manifold.** Illustration of a family of standard MEP models (right) and its deformed counterpart (bottom left). The space of MEP distributions with constraints of different orders constitute nested sub-manifolds [29], giving rise to a hierarchy of sub-families of models of the form $\mathcal{E}_k^\gamma = \{p_\gamma^{(k)}(\mathbf{x}) = e^{-\varphi_\gamma} [1 - \gamma\beta E_k(\mathbf{x})]_+^{1/\gamma}\}$ such that $\mathcal{E}_1^\gamma \subset \mathcal{E}_2^\gamma \subset \dots \subset \mathcal{E}_n^\gamma$ [42]. The foliation depends on the curvature γ , and in general $\mathcal{E}_k^\gamma \neq \mathcal{E}_k^0$ but rather $\mathcal{E}_k^\gamma \cap \mathcal{E}_r^0 \neq \emptyset$ for $k < r$. For small values of $|\gamma|$, it is possible to neglect higher-order terms in (4), and therefore certain subsets of \mathcal{E}_k^γ effectively approximate \mathcal{E}_r^0 .

machines [50]. Interestingly, these models can encode patterns in their weights in the form of ‘associative memories’ as in Nakano-Amari-Hopfield networks [51–53], being amenable for investigations using tools from equilibrium and nonequilibrium statistical physics literature [54–57]. Following the principles laid down in the previous section, we now introduce a family of recurrent neural networks that we call *curved neural networks*.

For this purpose, let us consider N binary variables x_1, \dots, x_N taking values in $\{1, -1\}$ following a joint probability distribution

$$p_\gamma(\mathbf{x}) = \exp(-\varphi_\gamma) [1 - \gamma\beta E(\mathbf{x})]_+^{1/\gamma}, \quad (5)$$

where φ_γ is a normalising constant. Above, we call $E(\mathbf{x})$ and β the (stochastic) *energy function* (i.e., Hamiltonian) and the *inverse temperature* due to their similarity with the Gibbs distribution in statistical physics when $\gamma \rightarrow 0$. Note that, unlike exponential families, these models do not exhibit energy invariance under constant shifts. However, as demonstrated in Ref. [41], deformed exponential models can be related to energy-invariant models by rescaling their temperature, which can be seen as maximizing entropy with respect to escort statistics rather than the original natural statistics.

Neural network models are typically defined by considering $p_\gamma(\mathbf{x})$ as defined in (5) with an energy function of the form

$$E(\mathbf{x}) = - \sum_{i=1}^N H_i x_i - \frac{1}{N} \sum_{i < j} J_{ij} x_i x_j, \quad (6)$$

where J_{ij} is the coupling strength between neurons x_i and x_j , and H_i are bias terms. In the limit $\gamma \rightarrow 0$, $p_0(\mathbf{x})$ recovers the Ising model. Emulating classical associative memories, the weights J_{ij} can be made to encode a collection of M neural patterns $\boldsymbol{\xi}^a = \{\xi_1^a, \dots, \xi_N^a\}$, $\xi_i^a = \pm 1$ and $a = 1, \dots, M$ by using the well-known Hebbian rule [53, 54]

$$J_{ij} = \sum_{a=1}^M \xi_i^a \xi_j^a. \quad (7)$$

Before proceeding with our main analysis, one can gain insights into the effect of the curvature γ from the dynamics of a recurrent neural network that behaves as a sampler of the equilibrium distribution described by (5). For this, we adapt the classic Glauber dynamics to curved neural networks (see Supplementary Note 2) to obtain

$$p(x_i | \mathbf{x}_{\setminus i}) = \left(1 + [1 - \gamma\beta'(\mathbf{x})\Delta E(\mathbf{x})]_+^{1/\gamma} \right)^{-1}, \quad (8)$$

where $\mathbf{x}_{\setminus i}$ denotes the state of all neurons except x_i , $\Delta E(\mathbf{x}) = 2(H_i + x_i \sum_j J_{ij} x_j)$ is the energy difference associated with detailed balance, and $\beta'(\mathbf{x})$ is an effective inverse temperature given by

$$\beta'(\mathbf{x}) = \frac{\beta}{[1 - \gamma\beta E(\mathbf{x})]_+}. \quad (9)$$

Again, $\gamma \rightarrow 0$ recovers the classic Glauber dynamics and $\beta'(\mathbf{x}) = \beta$. Thus, the curvature affects the dynamics through the deformed nonlinear activation function (8) and the state-dependent effective temperature $\beta'(\mathbf{x})$ (9), with high or low $\beta'(\mathbf{x})$ inducing higher or lower degrees of randomness in the transitions. The effect of $E(\mathbf{x})$ on $\beta'(\mathbf{x})$ depends then on the sign of γ . Negative γ increases effective temperature during relaxation, creating a positive feedback loop that accelerates convergence to low-energy state. The effect is similar to simulated annealing, but the coupling of the energy and effective temperature let the annealing scheduling to self-regulate. In contrast, positive γ decelerates the dynamics through negative feedback. Such accelerating or decelerating dynamics underlie non-trivial complex collective behaviours, which will be examined in the subsequent sections.

Mean-field behaviour of curved associative-memory networks

Mean-field solution

As with regular associative memories [56], one can solve the behaviour of curved associative-memory networks through mean-field methods in the thermodynamic limit $N \rightarrow \infty$ (Supplementary Note 3). Here the energy value of the model is extensive, meaning that it scales

with the system's size N . To ensure the deformation parameter remains independent of system properties such as size or temperature, we scale it as follows:

$$\gamma = \frac{\gamma'}{N\beta}. \quad (10)$$

Under this condition, we calculate the normalising potential φ_γ by introducing a delta integral and calculating a saddle-node solution, resulting in a set of order parameters $\mathbf{m} = \{m_1, \dots, m_M\}$, $m_a = \frac{1}{N} \sum_i \xi_i^a \langle x_i \rangle$ in the limit of size $N \rightarrow \infty$. This calculation assumes $1 - \gamma\beta E(\mathbf{x}) > 0$ so that $[\cdot]_+$ operators can be omitted and φ_γ is differentiable. The solution results in (for $H_i = 0$):

$$\begin{aligned} \varphi_\gamma = N \frac{\beta}{\gamma'} \log \frac{\beta'}{\beta} - \sum_{a=1}^M \beta' N m_a^2 \\ + \sum_{i=1}^N \log \left(2 \cosh \left(\beta' \sum_{a=1}^M \xi_i^a m_a \right) \right), \end{aligned} \quad (11)$$

where β' is given by

$$\beta' = \frac{\beta}{1 + \gamma' \frac{1}{2} \sum_a m_a^2}, \quad (12)$$

and the values of the mean-field variables m_a are found from the following self-consistent equations:

$$m_a = \sum_{i=1}^N \frac{\xi_i^a}{N} \tanh \left(\beta' \sum_{b=1}^M \xi_i^b m_b \right). \quad (13)$$

Similarly, using a generating functional approach [57], we use the Glauber rule in (8) to derive a dynamical mean-field given by path integral methods (see Supplementary Note 4). This yields

$$\dot{m}_a = -m_a + \sum_{i=1}^N \frac{\xi_i^a}{N} \tanh \left(\beta' \sum_{b=1}^M \xi_i^b m_b \right), \quad (14)$$

where β' is defined as in (12) for each \mathbf{m} . Note that in large systems, we recover the classical nonlinear activation function, and the deformation affects the dynamics only through the effective temperature β' .

Explosive phase transitions

To illustrate these findings, let us focus on a neural network with a single associative pattern ($M = 1$), similar to the Mattis model [58] and is equivalent to a homogeneous mean-field Ising model [59] (with energy $E(\mathbf{x}) = -\frac{1}{N} J \sum_{i < j} x_i x_j$) by using a variable change $x_i \leftarrow \xi_i x_i$. Rewriting (13), we find that a one-pattern curved neural network follows a mean-field model given by

$$m = \tanh(\beta' m), \quad (15)$$

$$\beta' = \frac{\beta}{1 + \gamma' \frac{1}{2} m^2}. \quad (16)$$

This result generalises the well-known Ising mean-field solution $m = \tanh(\beta J m)$, which is recovered when $\gamma = 0$.

By evaluating these equations, one finds that the model exhibits the usual order-disorder phase transition for positive and small negative values of γ' (Fig. 2.a top). However, for large negative values of γ' , a different behaviour emerges: an explosive phase transition [8] that displays hysteresis due to HOIs (Fig. 2.a bottom). The resulting phase diagram (Fig. 2.b) closely resembles phase transitions in higher-order contagion models [9, 11] and higher-order synchronisation observed in Kuramoto models [30].

a. Interpretation of the deformation parameter. One can intuitively interpret the effect of the deformation parameter γ' by noticing that, for a fixed β' , m is the solution of a function of β' . For $\gamma' = 0$, this results in the mean-field behaviour of the regular exponential model, which assigns a value of m to each inverse temperature $\beta = \beta'$. In the case of the deformed model, the possible pairs of solutions (m, β') are the same, but it changes their mapping to the inverse temperatures β . Namely, this deformation can be interpreted as a stretching (or contraction) of the effective temperature, which maps each pair (m, β') to an inverse temperature $\beta = \beta'(1 + \frac{1}{2} \gamma' J m^2)$ according to (16). Thus, one can obtain the mean-field solutions of the deformed patterns as mappings of the solutions of the original model. This is illustrated in Fig. 2.c, where the solution of β', m, β is projected to the planes $\beta = 0$ and $\beta' = 0$, obtaining the solutions for the flat ($\gamma' = 0$) and the deformed ($\gamma' = -1.2$) models respectively.

b. Explosive dynamics. In order to gain a deeper understanding of the explosive nature of this phase transition, we study the dynamics of the single-pattern neural network. By rewriting (14) for $M = 1$, and under the change of variables mentioned above to remove ξ , the dynamical mean-field equation of the system reduces to

$$\dot{m} = -m + \tanh(\beta' m), \quad (17)$$

where β' is calculated as in (16). Simulations of the dynamical mean-field equations for values of β just above the critical point are depicted in Fig. 2.d. Trajectories with strongly negative γ' saturate earlier than smaller negative γ' , confirming accelerated convergence. During this process, the effective inverse temperature β' rapidly increases until it saturates, making the dynamics less stochastic. Less stochastic dynamics lead to faster convergence of m , which in turn increases β' , creating a positive feedback loop between β' and m that gives rise to the explosive nature of the phase transition. This positive loop occurs only if γ' is negative; otherwise, negative feedback simply makes the convergence of m slower.

Overlaps between memory basins of attraction

A key property of associative-memory networks is their ability to retrieve patterns in different contexts. In the

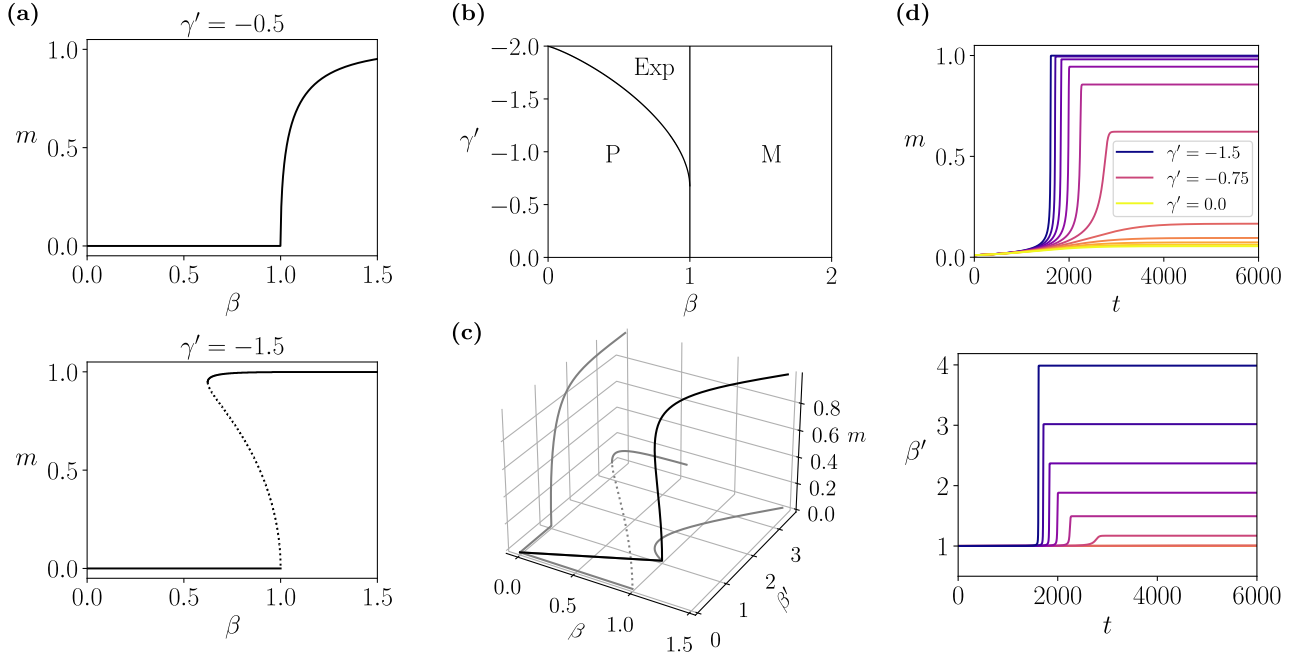


FIG. 2. **Explosive phase transitions in curved neural networks.** (a) Phase transitions of the curved neural network with one associative memory, for values of $\gamma' = -0.5$ (top, displaying a second-order phase transition) and $\gamma' = -1.5$ (bottom, displaying an explosive phase transition). Solid lines represent the stable fixed points, and dotted lines correspond to unstable fixed points. (b) Phase diagram of the system. The areas indicated by 'P' and 'M' refer to the usual paramagnetic (disordered) and magnetic (ordered) phases, respectively. The area indicated by 'Exp' represents a phase where ordered and disordered states coexist in an explosive phase transition characterised by a hysteresis loop. (c) Solution of Eqs. (15)-(16) for β', m, β (black line) for $\gamma' = -1.2$, and projections to the plane $m = 0$, $\beta = 0$ and $\beta' = 0$, obtaining respectively the relation between β, β' and solutions of the flat and the deformed models respectively (grey lines). (d) Mean-field dynamics of the single-pattern neural network for $\beta = 1.001$ (near criticality from the ordered phase) for some values of γ' in $[-1.5, 0]$. For large negative γ' the dynamics 'explodes', with m (top) and β' (bottom) converging abruptly.

case of one-pattern associative-memory networks, the energy function $E(\mathbf{x}) = -\sum_{i<j} x_i \xi_i \xi_j x_j$ is a quadratic function with two minima at $\mathbf{x} = \pm \boldsymbol{\xi}$, which act as global attractors. Instead, a two-pattern associative-memory network has an energy function with four minima (if sufficiently separated), but their attraction basins overlap when the patterns are correlated.

To study the degree of the overlap between pairs of patterns, we analyse solutions of (13) for a network with two patterns with correlation $\langle \xi_i^1 \xi_i^2 \rangle = C$ (see Supplementary Note 3.3 for details). In this scenario, the system is described by two mean field patterns:

$$m_a = \frac{1}{2}(1 + C) \tanh(\beta'(m_1 + m_2)) + w \frac{1}{2}(1 - C) \tanh(\beta'(m_1 - m_2)), \quad (18)$$

with $w = 3 - 2a = \pm 1$ for $a = 1, 2$ and

$$\beta' = \frac{\beta}{1 + \gamma \frac{1}{2}(m_1^2 + m_2^2)}. \quad (19)$$

Fig. 3 shows how the hysteresis effect and explosive phase transitions persist in the case of two patterns for $C = 0.2$ with negative γ' . This example shows two consecutive, overlapping explosive bifurcations (going from

1 to 2, and then to 4 fixed points), creating a hysteresis involving 7 fixed points within a more compressed parameter range of β than the classical case. Consequently, the memory-retrieval region for the four embedded memories expands. These results illustrate complex hysteresis cycles as well as an increased memory capacity for finite temperatures by negative values of γ' . This enhanced capability for memory retrieval is further investigated through the analyses presented in the next section.

Memory retrieval with an extensive number of patterns

Next, we sought to investigate how the deformation related to γ impacts the memory-storage capacity of associative memories. In classical associative networks of N neurons, the energy function is defined as $E(\mathbf{x}) = -\frac{1}{N} \sum_{a=1}^M \sum_{i<j} x_i \xi_i^a \xi_j^a x_j$, taking $M = \alpha N$ as the number of patterns learned by the network transforms the system into a disordered spin model in the thermodynamic limit. Furthermore, one can analytically solve this model [60–63]. For example, using the replica-trick method can determine the memory capacity of the system [60], and theoretically identify the critical value of α

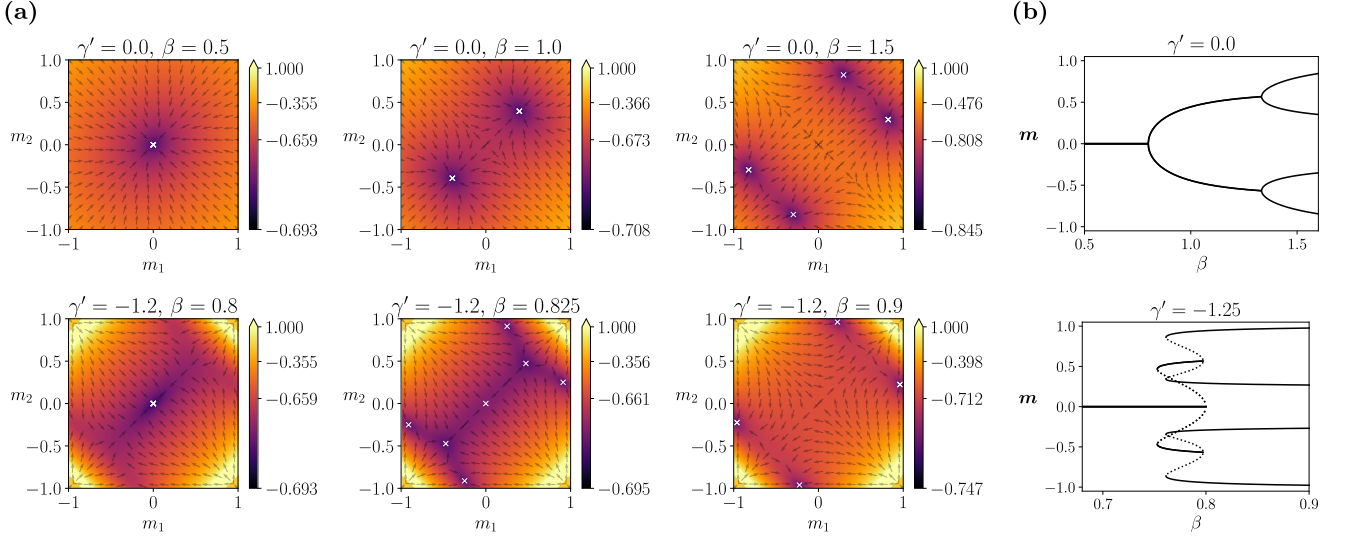


FIG. 3. **Interaction between two encoded memories.** (a) Values of φ_γ for different mean-field values m_1, m_2 , indicating the attractor structure of the network for different values of β with $C = 0.2$ for $\gamma' = 0$ (top row) and $\gamma' = -1.2$ (bottom row). (b) Bifurcations of the order parameters m_1, m_2 . For $\gamma' = 0$ we observe an attractor bifurcating into two and then into four. For $\gamma' = -1.2$, we observe the same sequence, but with a coexistence hysteresis regime in which 7 attractors are possible.

at which memory retrieval becomes impossible — leading to a disordered spin-glass phase. Here, we apply a similar approach to reveal how deformed associative memory networks afford an enhanced memory capacity.

Applying the replica trick in conjunction with the methods outlined in previous sections allows us to solve the system using φ_γ for the deformed exponential (see Supplementary Note 5). This method entails computing a mean-field variable m corresponding to one of the patterns ξ^a and averaging over the others. For simplicity, a pattern with all positive unity values $\xi^a = (1, 1, \dots, 1)$ is considered, which is equivalent to any other single pattern just by a series of sign flip variable changes. The degree of similarity or overlap of this pattern with other patterns in the system introduces a new order parameter q , which contributes to measuring disorder in the system. After introducing the relevant order parameters and solving under a replica-symmetry assumption, the normalising potential is derived as

$$\begin{aligned} \varphi_\gamma = & N \frac{\beta}{\gamma'} \log \frac{\beta}{\beta'} - N \beta' J m^2 - N \frac{1}{2} \alpha (\beta' J)^2 (r + R - 2qr) \\ & - N \frac{1}{2} \alpha (\log(1 - \beta' J(1 - q)) - \beta' J \sqrt{r q}) \\ & + N \int Dz \log(2 \cosh(\beta' J m + \beta' J \sqrt{\alpha r} z)), \end{aligned} \quad (20)$$

where J is a scaling factor and order parameters are defined as

$$m = \int Dz \tanh(\beta' J m + \beta' J \sqrt{\alpha r} z), \quad (21)$$

$$q = \int Dz \tanh^2(\beta' J m + \beta' J \sqrt{\alpha r} z), \quad (22)$$

with

$$r = \frac{q}{(1 - \beta' J(1 - q))^2}, \quad R = \frac{(\beta' J)^{-1} - (1 - 2q)}{(1 - \beta' J(1 - q))^2}. \quad (23)$$

As in previous cases, the model is governed by an effective temperature

$$\beta' = \frac{\beta}{1 + \gamma' \frac{1}{2} (J m^2 + \alpha J (\beta' (R - qr) - 1))}. \quad (24)$$

This solution differs from the models in previous sections by the self-dependence of β' .

To obtain a phase diagram, we solved Eqs. (21-22) numerically for given α, β' at $\gamma' = 0$, and rescaled the inverse temperature as in the previous step to obtain the corresponding values of β for each γ' . Using the resulting order parameters and calculating the free energy for each α, β, γ' , we constructed the phase diagram of the system (similarly to [56, 60]) characterised by the following distinct phases (Fig. 4):

- A disordered phase (P) with $m = q = 0$.
- A ferromagnetic phase (F), corresponding to stable memory-retrieval solutions with $m > 0$ and $q > 0$.
- A spin-glass phase (SG), exhibiting spurious-retrieval solutions where $m = 0$ and $q > 0$.
- A mixed phase (M), where F and SG types of solutions coexist, being the spin-glass solutions a global minimum of the normalizing potential φ_γ .

For $\gamma' = 0$ (black dashed lines), the phase transition reflects the behaviour of associative memories near saturation [56, 60]. With negative γ' (red lines), we observe

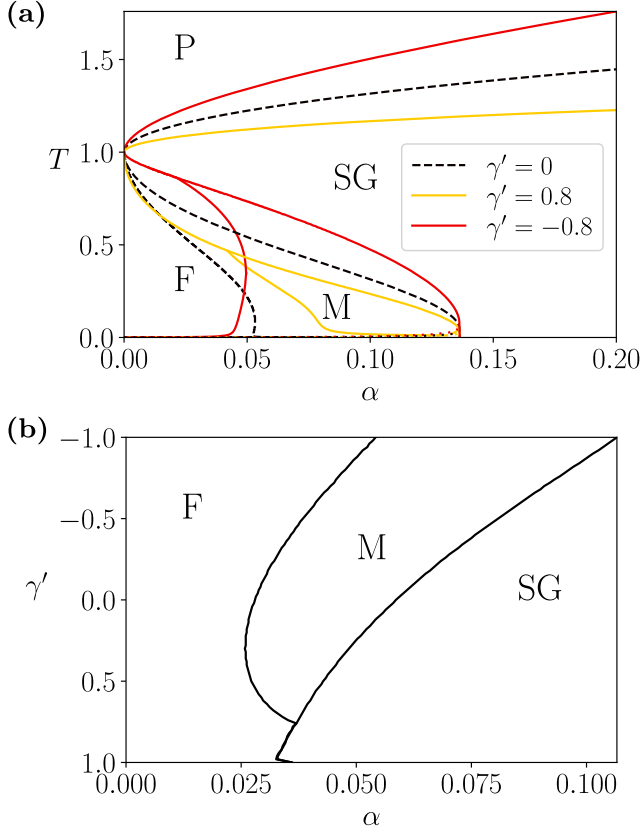


FIG. 4. Memory capacity is enhanced by geometric deformation. Phase diagram of a curved associative memory with an extensive number of encoded patterns $M = \alpha N$ for (a) different $T = 1/\beta$ at $\gamma' = 0$ (black dashed lines), 0.8, -0.8 (solid lines), and for (b) different γ' at $\beta = 2$. F indicates the ferromagnetic (i.e., memory retrieval) phase, SG the spin-glass phase (where saturation makes memory retrieval inviable), M a mixed phase, and P the paramagnetic region. Both in F and M, ferromagnetic and spin-glass solutions coexist, but we differentiate these by calculating respectively whether memory-retrieval or spin-glass solutions are the global minimum of the normalizing potential φ_γ . The dotted lines in (a) near $T = 0$ indicate the AT lines, below which the replica solution is not valid. Increasing γ' to larger negative values extends the retrieval phase into larger values of α , indicating an increased memory capacity, while larger positive values reduce the extension of the mixed phase, increasing robustness of memory retrieval.

an expansion of the ferromagnetic and mixed phases, indicating an enhanced memory-storage capacity by the deformation. Conversely, a positive value of γ' (yellow lines) decreases the memory capacity but reduces the extent of the mixed phase. In the mixed phase, retrieved memories ($m > 0$) are represented at a local — but not global — minimum of the normalising potential φ_γ in (20), indicating a larger probability of observing spurious patterns. Thus, we expect positive values of γ' to result in more robust memory retrieval.

The stability of the replica symmetry solution is given

by the condition

$$(1 + \beta'(1 - q))^2 > \alpha\beta'^2 \int Dz \cosh^{-4} \beta' (Jm + J\sqrt{\alpha}rz), \quad (25)$$

which is captured by the dotted lines near zero temperature in Fig. 4.a. Note that all solutions in Fig. 4.b are stable under the replica symmetry assumption.

a. Experimental validation We complement the analysis from the previous section with an experimental study of a system encoding patterns from an image classification benchmark. The patterns are sourced from the CIFAR-100 dataset, which comprises 60,000 32x32 colour images [64]. To adapt the dataset to binary patterns suitable for storage in an associative memory, we processed each RGB channel by assigning a value of 1 to pixels with values greater than the channel's median value and -1 otherwise (Fig. 5.a). The resulting array of $N = 32 \cdot 32 \cdot 3$ binary values for each image was assigned to patterns ξ^a . Note that associative memories (as well as our theory above) usually assume that patterns are relatively uncorrelated, and specific methods are required to adapt them to correlated patterns [65, 66]. To simplify the problem, we conducted experiments using a selection of 100 images with covariance values smaller than $10/\sqrt{N}$ (the standard deviation of covariance values for uncorrelated patterns is $1/\sqrt{N}$). We used a random search to select patterns with low correlations: we randomly picked an image and replaced it if its correlation exceeded the threshold, repeating until all correlations were below it.

We evaluate the memory retrieval capacity of networks with various degrees of curvature γ by encoding different numbers of memories, as described in (7). As a measure of performance, we evaluated the stability of the network by assigning an initial state $\mathbf{x} = \xi^a$ and calculating the overlap $o = \sum_i x_i \xi_i^a$ after $T = 30N$ Glauber updates. The process was repeated $R = 500$ times from different initial conditions (different encoded patterns and different initial states) to estimate the value of m in (21). Experimental outcomes confirm our theoretical results, revealing that memory capacity increases with negative values of γ' , while positive values reduce the memory capacity (Fig. 5.b), but reduce the extent and magnitude of the high variability region in pattern retrieval, which is consistent with the reduction of the mixed phase (Fig. 5.c). Note that the resulting memory capacity of the system observed in our experiments (i.e., the value of α at which the transition happens) is diminished due to the presence of correlations among some of the memorised patterns.

b. Explosive spin-glass transition For $J \rightarrow 0$ and $\alpha = J^{-2}$, the model converges to (see Supplementary

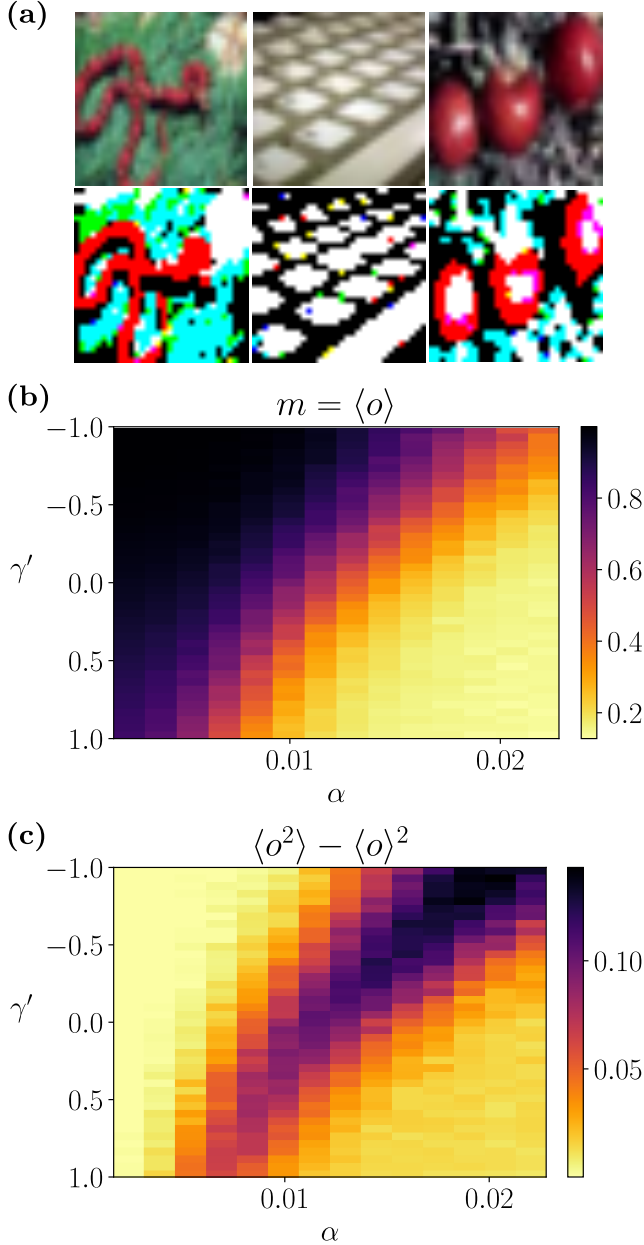


FIG. 5. **Simulation study for the effect of deformation on image encoding.** (a) Examples of CIFAR-100 images (top) and their RGB binarised versions (bottom). Every $32 \times 32 \times 3$ binary RGB pixel value for each image a is assigned to the value of one position of pattern ξ_i^a . (b, c) Mean and variance of pattern retrieval values obtained in experiments, measured by the overlap between the final state of the network and the encoded pattern.

Notes 5)

$$q = \int Dz \tanh^2(\beta' \sqrt{q} z), \quad (26)$$

$$\beta' = \frac{\beta}{1 + \frac{1}{2} \gamma' \beta' (1 - q^2)}, \quad (27)$$

which at $\gamma = 0$ recovers the well-known Sherrington-Kirkpatrick model [67]. While in the classical case, a phase transition occurs from a paramagnetic to a spin-glass phase, the curvature effect of $\gamma' \neq 0$ introduces novel phase transitions. For small values of γ' , the system exhibits a continuous phase transition akin to the Sherrington-Kirkpatrick spin-glass, where $\frac{dq}{d\beta}$ shows a cusp (Fig. 6.a). However, for $\gamma' = -1$ the phase transition becomes second-order, displaying a divergence of $\frac{dq}{d\beta}$ at the critical point (Fig. 6.b). Moreover, increasing the magnitude of negative γ' leads to a first-order phase transition with hysteresis (Fig. 6.c), resembling the explosive phase transition observed in the single-pattern associative-memory network. This hybrid phase transition combines the typical critical divergence of a second-order phase transition with a genuine discontinuity, similar to ‘type V’ transitions as described in [8].

We analytically calculated the properties of these phase transitions (see Supplementary Note 6). By computing the solution at $\gamma' = 0$ and rescaling β' , we determined that the critical point is located at $\beta_c = 1 + \frac{1}{2} \gamma'$ (consistent with Fig. 6.a-c). The slope of the order parameter around the critical point is, for $\gamma' < 1$, equal to $(1 + \gamma')^{-1}$, indicating the onset of a second-order phase transition as depicted in Fig. 6.b. The resulting phase diagram of the curved Sherrington-Kirkpatrick model is shown in Fig. 6.d.

DISCUSSION

HOIs play a critical role in enabling emergent collective phenomena in natural and artificial systems. Modelling HOIs is, however, highly non-trivial, often requiring advanced analytic tools (such as hypergraphs and simplicial complexes) that entail an exponential increase in parameters for large systems. Here we address this issue by leveraging the maximum entropy principle to effectively capture HOIs in models via a deformation parameter γ , which is associated with the Rényi entropy. Given their close connection with statistical physics, this family of models provides a useful setup to investigate the effect of HOIs on spin systems, including explosive ferromagnetic and spin-glass phase transitions, extending studies on anomalous phase transitions found in other systems [2, 7–9, 11], and the capability of networks to store memories.

Although our primary objective is to develop a parsimonious model of HOIs to explain higher-order phenomena, our framework is broadly applicable to explain the behaviour of dense associative networks with HOIs, including recently proposed relativistic Hopfield model [32–34]. To explain this, let us consider the energy $\mathcal{F}[E]$ of the exponential family distribution $p(\mathbf{x}) \sim e^{-\beta \mathcal{F}[E]}$ given by the nonlinear transformation (denoted by \mathcal{F}) of the classical energy $E(\mathbf{x})$. The deformed exponential models studied in this paper correspond to $\mathcal{F}[E] = -\frac{N}{\gamma'} \log(1 - \gamma' E/N)$, while the relativistic model corre-

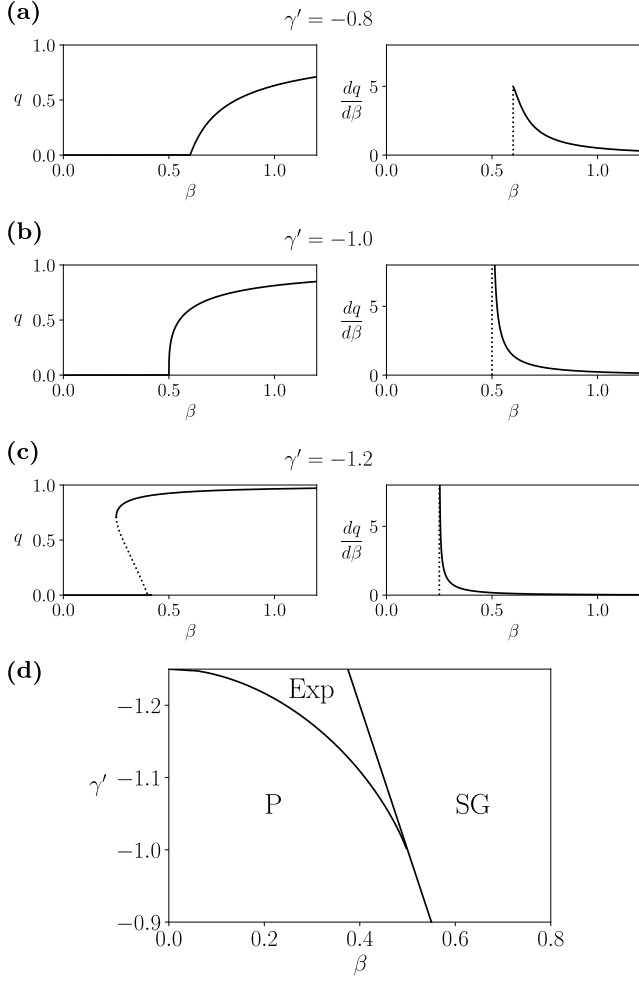


FIG. 6. **Explosive spin glasses.** Phase transitions for order parameter q for replica-symmetric disordered spin models displaying (a) a cusp phase transition for $\gamma' = -0.5$, (b) a second-order phase transition for $\gamma' = -1.0$ and (c) an explosive phase transition for $\gamma' = -1.2$. (d) Phase diagram of the explosive spin glass, displaying a paramagnetic (P), spin-glass (SG) and an explosive phase (Exp).

spond to $\mathcal{F}[E] = -\frac{N}{\gamma'} \sqrt{1 - \gamma' E/N}$. For the deformed exponential, the term $\mathcal{F}[E]$ can be expanded as

$$\mathcal{F}[E] = E + \frac{\gamma'}{2N} E^2 + \frac{\gamma'^2}{3N^2} E^3 + \dots \quad (28)$$

When E depends on the quadratic Mattis magnetisation (i.e., $E = -\sum_a \frac{1}{N} (\sum_i \xi_i^a x_i)^2$), then $\mathcal{F}[E]$ expands in terms of even-order HOIs of $\sum_i \xi_i^a x_i$. The same signs appear for each order in the relativistic energy with $\gamma' < 0$. For $\gamma' < 0$, all coefficients of $\sum_i \xi_i^a x_i$ in the expansion are negative, indicating that embedded memories have deeper energy minima than the classical case. We also note that β in the free energy of both the deformed exponential and relativistic models in the limit of large N appears scaled according to an effective temperature given by $\beta' = \beta \partial_E \mathcal{F}[E]$ (e.g., (11) and Eq. 6.2

in Ref. [34]). Moreover, the input in the Glauber dynamics is approximated for large sizes as $\beta \Delta \mathcal{F}[E] \approx \beta \partial_E \mathcal{F}[E] \Delta E(\mathbf{x}) = \beta' \Delta E(\mathbf{x})$. The effective inverse temperatures $\beta' = \beta(1 - \gamma' E/N)^{-1}$ for the deformed exponential and $\beta' = 2^{-1}(1 - \gamma' E/N)^{-1/2}$ for the relativistic models become larger for negative E when $\gamma' < 0$, resulting in an acceleration of memory retrieval. While the relativistic model has been studied for $\gamma' > 0$ [32–34], we conjecture it may exhibits explosive phase transitions if $\gamma' < 0$. Conversely, a positive γ' introduces even-order terms of $\sum_i \xi_i^a x_i$ with alternating-signs and a shallower energy landscape due to a reduction in β' . This shallower energy landscape diminishes the memory capacity by expanding the spin-glass phases (Fig. 4), but also enlarges the recall (ferromagnetic) region by mitigating the formation of spurious memories given by overlapping patterns in the mixed phase.

These findings underscore the distinct roles of HOIs in memory retrieval, deepening our understanding of the mechanisms at play while opening the door for future extensions harnessing these new intuitions. This perspective, based on the self-regulated annealing and scaling of β , can be extended to dense associative memories [20, 21], which achieve supralinear (e.g., polynomial or exponential) memory capacities by applying nonlinear transformations to each encoded pattern. Such nonlinearity narrows the basins of attraction of individual memories, reducing overlap and preventing the spin-glass phase. In this way, the memory capacity of these models is engineered to be much higher than the results in this paper. Nevertheless, we hypothesise that dense associative memories can be *curved* using techniques similar to the ones developed here. Although this goes beyond the scope of this paper, exploring whether such curvature can further enhance memory capacity offers a compelling direction for future research.

Curved neural networks also provide insights into biological neural systems, where evidence suggests the presence of alternating positive and negative HOIs for even and odd order, respectively. This alternation leads to sparse neuronal activity, which has been shown to be instrumental for enabling extended periods of total silence [5, 13–15, 35]. The realisation of dense associative memories, combined with sparse population activity, represents a significant avenue for achieving energy efficiency in modern machines [35, 36]. Interestingly, such sparse activities may coexist with the accelerated memory retrieval dynamics, as both may involve positive even-order HOIs. Future work may explore how curved neural networks might achieve both energy efficiency and high memory capacities, potentially by incorporating the effect of a negative bias term in the model. Additionally, developing statistical methods for fitting these models to experimental data (i.e., theories for learning) represents a promising yet still unexplored research avenue. These research directions constitute a promising avenue to investigate the principles underlying efficient information coding in biological neural systems.

Overall, our results demonstrate the benefits of considering the maximum entropy principle, emergent HOIs, and nonlinear network dynamics as theoretically intertwined notions. As showcased here, such an integrated framework reveals how information encoding, retrieval dynamics, and memory capacity in neural networks are mediated by HOIs, enabling principled, analytically tractable tools and insights from statistical mechanics and nonlinear dynamics. More generally, the framework presented in this paper extends beyond neural networks and contributes to a general theory of HOIs, paving the road towards a principled study of higher-order phenomena in complex networks.

DATA AVAILABILITY

The CIFAR-100 dataset used in this study is available at <https://www.cs.toronto.edu/~kriz/cifar.html>

CODE AVAILABILITY

The code generated in this study is available in the GitHub repository, <https://github.com/MiguelAguilera/XXXX>.

-
- [1] R. Lambiotte, M. Rosvall, and I. Scholtes, *Nature physics* **15**, 313 (2019).
 - [2] F. Battiston, E. Amico, A. Barrat, G. Bianconi, G. Ferraz de Arruda, B. Franceschiello, I. Iacopini, S. Kéfi, V. Latora, Y. Moreno, *et al.*, *Nature Physics* **17**, 1093 (2021).
 - [3] S.-i. Amari, H. Nakahara, S. Wu, and Y. Sakai, *Neural computation* **15**, 127 (2003).
 - [4] C. Kuehn and C. Bick, *Science advances* **7**, eabe3824 (2021).
 - [5] S. R. Shomali, S. N. Rasuli, M. N. Ahmadabadi, and H. Shimazaki, *Communications Biology* **6**, 169 (2023).
 - [6] V. Thibault, A. Allard, and P. Desrosiers, *Nature Physics* **20**, 294 (2024).
 - [7] S. Angst, S. R. Dahmen, H. Hinrichsen, A. Hucht, and M. P. Magiera, *Journal of Statistical Mechanics: Theory and Experiment* **2012**, L06002 (2012).
 - [8] R. M. D'Souza, J. Gómez-Gardenes, J. Nagler, and A. Arenas, *Advances in Physics* **68**, 123 (2019).
 - [9] I. Iacopini, G. Petri, A. Barrat, and V. Latora, *Nature communications* **10**, 2485 (2019).
 - [10] A. P. Millán, J. J. Torres, and G. Bianconi, *Physical Review Letters* **124**, 218301 (2020).
 - [11] N. W. Landry and J. G. Restrepo, *Chaos: An Interdisciplinary Journal of Nonlinear Science* **30** (2020).
 - [12] F. Montani, R. A. Ince, R. Senatore, E. Arabzadeh, M. E. Diamond, and S. Panzeri, *Philosophical Transactions of the Royal Society A: Mathematical, Physical and Engineering Sciences* **367**, 3297 (2009).
 - [13] G. Tkačik, O. Marre, D. Amodei, E. Schneidman, W. Bialek, and M. J. Berry, *PLoS computational biology* **10**, e1003408 (2014).
 - [14] I. E. Ohiorhenuan, F. Mechler, K. P. Purpura, A. M. Schmid, Q. Hu, and J. D. Victor, *Nature* **466**, 617 (2010).
 - [15] H. Shimazaki, K. Sadeghi, T. Ishikawa, Y. Ikegaya, and T. Toyoizumi, *Scientific reports* **5**, 9821 (2015).
 - [16] G. Tkačik, O. Marre, T. Mora, D. Amodei, M. J. Berry II, and W. Bialek, *Journal of Statistical Mechanics: Theory and Experiment* **2013**, P03011 (2013).
 - [17] G. Tkačik, T. Mora, O. Marre, D. Amodei, S. E. Palmer, M. J. Berry, and W. Bialek, *Proceedings of the National Academy of Sciences* **112**, 11508 (2015).
 - [18] T. F. Burns and T. Fukai, in *The Eleventh International Conference on Learning Representations* (2022).
 - [19] C. Bybee, D. Kleyko, D. E. Nikonov, A. Khosrowshahi, B. A. Olshausen, and F. T. Sommer, *Nature Communications* **14**, 6033 (2023).
 - [20] D. Krotov and J. J. Hopfield, *Advances in neural information processing systems* **29** (2016).
 - [21] M. Demircigil, J. Heusel, M. Löwe, S. Upgang, and F. Vermet, *Journal of Statistical Physics* **168**, 288 (2017).
 - [22] E. Agliari, L. Albanese, F. Alemanno, A. Alessandrelli, A. Barra, F. Giannotti, D. Lotito, and D. Pedreschi, *Physica A: Statistical Mechanics and its Applications* **627**, 129143 (2023).
 - [23] C. Lucibello and M. Mézard, *Physical Review Letters* **132**, 077301 (2024).
 - [24] D. Krotov, *Nature Reviews Physics* **5**, 366 (2023).
 - [25] L. Ambrogioni, *Entropy* **26**, 381 (2024).
 - [26] L. Ambrogioni, *arXiv preprint arXiv:2310.17467* (2023).
 - [27] A. Bovier and B. Niederhauser, *arXiv preprint cond-mat/0108235* (2001).
 - [28] E. Agliari, A. Fachechi, and C. Marullo, *Journal of Mathematical Physics* **63** (2022).
 - [29] S.-i. Amari, *IEEE transactions on information theory* **47**, 1701 (2001).
 - [30] P. S. Skardal and A. Arenas, *Communications Physics* **3**, 218 (2020).
 - [31] E. Ganmor, R. Segev, and E. Schneidman, *Proceedings of the National Academy of sciences* **108**, 9679 (2011).
 - [32] A. Barra, M. Beccaria, and A. Fachechi, *Neural Networks* **106**, 205 (2018).
 - [33] E. Agliari, A. Barra, and M. Notarnicola, *Journal of Mathematical Physics* **60** (2019).
 - [34] E. Agliari, F. Alemanno, A. Barra, and A. Fachechi, *Neural Networks* **128**, 254 (2020).
 - [35] U. Rodríguez-Domínguez and H. Shimazaki, *arXiv preprint arXiv:2308.13257* (2023).
 - [36] S. Santos, V. Niculae, D. McNamee, and A. F. Martins, *arXiv preprint arXiv:2411.08590* (2024).
 - [37] B. Hoover, D. H. Chau, H. Strobelt, P. Ram, and D. Krotov, *arXiv preprint arXiv:2410.24153* (2024).
 - [38] E. T. Jaynes, *Probability theory: The logic of science* (Cambridge university press, 2003).
 - [39] R. Cofré, R. Herzog, D. Corcoran, and F. E. Rosas, *Entropy* **21**, 1009 (2019).
 - [40] E. T. Jaynes, *Physical review* **106**, 620 (1957).
 - [41] C. Tsallis, R. Mendes, and A. R. Plastino, *Physica A: Statistical Mechanics and its Applications* **261**, 534 (2000).

- (1998).
- [42] P. A. Morales and F. E. Rosas, *Phys. Rev. Res.* **3**, 033216 (2021).
 - [43] F. Valverde-Albacete and C. Peláez-Moreno, *Entropy* **21**, 46 (2019).
 - [44] S. Umarov, C. Tsallis, and S. Steinberg, *Milan journal of mathematics* **76**, 307 (2008).
 - [45] N. Guisande and F. Montani, *Frontiers in Computational Neuroscience* **18**, 1342985 (2024).
 - [46] M. Jauregui, L. Zunino, E. K. Lenzi, R. S. Mendes, and H. V. Ribeiro, *Physica A: Statistical Mechanics and its Applications* **498**, 74 (2018).
 - [47] R. F. Vigelis, L. H. De Andrade, and C. C. Cavalcante, *IEEE Transactions on Information Theory* **66**, 2891 (2019).
 - [48] S.-i. Amari, *Information geometry and its applications*, Vol. 194 (Springer, 2016).
 - [49] Y. Roudi, B. Dunn, and J. Hertz, *Current opinion in neurobiology* **32**, 38 (2015).
 - [50] G. Montúfar, in *Information Geometry and Its Applications: On the Occasion of Shun-ichi Amari's 80th Birthday, IGAIA IV Liblice, Czech Republic, June 2016* (Springer, 2018) pp. 75–115.
 - [51] K. Nakano, *IEEE Transactions on Systems, Man, and Cybernetics* **3**, 380 (1972).
 - [52] S.-I. Amari, *IEEE Transactions on computers* **100**, 1197 (1972).
 - [53] J. J. Hopfield, *Proceedings of the national academy of sciences* **79**, 2554 (1982).
 - [54] D. J. Amit, *Modeling brain function: The world of attractor neural networks* (Cambridge university press, 1989).
 - [55] A. C. Coolen, R. Kühn, and P. Sollich, *Theory of neural information processing systems* (OUP Oxford, 2005).
 - [56] A. Coolen, in *Handbook of biological physics*, Vol. 4 (Elsevier, 2001) pp. 553–618.
 - [57] A. Coolen, in *Handbook of biological physics*, Vol. 4 (Elsevier, 2001) pp. 619–684.
 - [58] D. Mattis, *Physics Letters A* **56**, 421 (1976).
 - [59] M. Kochmański, T. Paszkiewicz, and S. Wolski, *European Journal of Physics* **34**, 1555 (2013).
 - [60] D. J. Amit, H. Gutfreund, and H. Sompolinsky, *Physical Review Letters* **55**, 1530 (1985).
 - [61] A. Bovier, V. Gayrard, and P. Picco, *Journal of statistical physics* **79**, 395 (1995).
 - [62] M. Talagrand, *Probability theory and related fields* **110**, 177 (1998).
 - [63] M. Shcherbina and B. Tirozzi, *Journal of statistical physics* **72**, 113 (1993).
 - [64] A. Krizhevsky, University of Toronto (2009).
 - [65] J. F. Fontanari and W. Theumann, *Journal de Physique* **51**, 375 (1990).
 - [66] E. Agliari, A. Barra, A. De Antoni, and A. Galluzzi, *Neural Networks* **38**, 52 (2013).
 - [67] D. Sherrington and S. Kirkpatrick, *Physical review letters* **35**, 1792 (1975).

ACKNOWLEDGMENTS

We thank Ulises Rodriguez Dominguez for valuable discussions on this manuscript. MA is funded by a Junior Leader fellowship from ‘la Caixa’ Foundation (ID 100010434, code LCF/BQ/PI23/11970024),

John Templeton Foundation (grant 62828), Basque Government ELKARTEK funding (code KK-2023/00085) and Grant PID2023-146869NA-I00 funded by MICIU/AEI/10.13039/501100011033 and cofunded by the European Union, and supported by the Basque Government through the BERC 2022-2025 program and by the Spanish State Research Agency through BCAM Severo Ochoa excellence accreditation CEX2021-01142-S funded by MICIU/AEI/10.13039/501100011033. P.A.M. acknowledges support by JSPS KAKENHI Grant Number 23K16855, 24K21518. H.S. is supported by JSPS KAKENHI Grant Number JP 20K11709, 21H05246, 24K21518.

CONTRIBUTIONS

M.A., P.A.M, F.E.R and H.S. designed and reviewed the research and wrote the paper. M.A. contributed the analytical and numerical results. P.A.M. contributed part of the analytical results of the replica analysis.

COMPETING INTERESTS

The authors declare no competing interests.

Explosive neural networks via higher-order interactions in curved statistical manifolds

Supplementary Information

Miguel Aguilera

*BCAM – Basque Center for Applied Mathematics, Bilbao, Spain
IKERBASQUE, Basque Foundation for Science, Bilbao, Spain*

Pablo A. Morales

*Research Division, Araya Inc., Tokyo, Japan
Centre for Complexity Science, Imperial College London, London, UK*

Fernando E. Rosas

*Department of Informatics, University of Sussex, Brighton, UK
Sussex Centre for Consciousness Science and Sussex AI, University of Sussex, Brighton, UK
Department of Brain Science, Imperial College London, London, UK
Center for Eudaimonia and Human Flourishing, University of Oxford, Oxford, UK*

Hideaki Shimazaki

*Graduate School of Informatics, Kyoto University, Kyoto, Japan
Center for Human Nature, Artificial Intelligence,
and Neuroscience (CHAIN), Hokkaido University, Sapporo, Japan***Supplementary Note 1: Maximum Rényi entropy and Information Geometry**

The maximum entropy principle (MEP) is a framework for building parsimonious models consistent with observations, being particularly well-suited for the statistical description of systems in contexts of incomplete knowledge [38, 39]. The MEP uses entropy as a fundamental tool to quantify the degree of structure present in a given model. Accordingly, the MEP suggest to adopt the model with the maximal entropy — i.e. the least amount of structure — that is compatible with a given set of observations, following the idea that one should not include regularities that are not contained in the data.

Maximum entropy models are particularly well-suited for the study of neural systems. By abstracting neurons into binary variables x_k representing the presence or absence of action potentials, the MEP provides a powerful approach to model collective neural activity. In this approach, the Ising model emerges from the maximisation of Shannon entropy under constraints on activity rates of individual neurons and pairwise correlations:

$$p^{(2)} = \arg \max_{q(\mathbf{x})} H(\mathbf{x}) \quad \text{s.t.} \quad \begin{cases} \langle x_i \rangle &= \eta_i, \\ \langle x_i x_j \rangle &= \eta_{ij}, \end{cases}$$

where $H(\mathbf{x})$ denotes the Shannon entropy of $\mathbf{x} = \{x_1, \dots, x_n\}$ under distribution $q(\mathbf{x})$. It can be shown that

$$p^{(2)}(\mathbf{x}) = \frac{1}{Z} \exp \left(\sum_i \theta_i x_i + \sum_{i < j} \theta_{ij} x_i x_j \right), \quad (\text{S1.1})$$

with Z being a normalising constant. Hence, this model encapsulates observed information up to second-order statistics, represented in how θ_i, θ_{ij} depend on the constraints η_i, η_{ij} . Furthermore, the dynamics of the Ising model can be investigated via exact solutions, approximations (encompassing mean-field and Bethe approximations), and simulations, thereby providing a rich set of insights and analytical tools. The Ising model has been instrumental in the development of recurrent neural networks, leading to Hopfield networks and Boltzmann machines.

What if the observations that one is to model require us to consider statistics beyond pairwise interactions? Following the same principle, one can construct models with third- and higher-order interactions [29] resulting on distributions of the following type:

$$p^{(k)}(\mathbf{x}) = \frac{1}{Z} \exp \left(\sum_{\substack{I \subseteq \{1, \dots, n\} \\ |I| \leq k}} \theta_I \prod_{i \in I} x_i \right) \quad (\text{S1.2})$$

with the summation going over all subsets of k or less variables. Above, the argument within the exponential is an energy function $E_k(\mathbf{x})$, with the index k highlighting the highest order of interactions considered. It is important to notice that the number of terms in the Hamiltonian grows exponentially with k , making unfeasible in practice to construct models including high orders $k \gg 1$.

1. Capturing high-order interactions via non-Shannon entropies

While traditional formulations of the MEP are based on Shannon's entropy [40], more recent work has expanded it to include other entropy functionals including the entropies of Tsallis [41] and Rényi [42]. Here we argue that some high-order interdependencies can be efficiently captured by the deformed exponential family (2), which arises as a solution to the problem of maximising non-Shannon entropies — as explained below.

By starting from a conventional MEP model with few degrees of freedom tuned to account for low-order interactions, one can enhance its capability to account for higher-order interdependencies by the inclusion of a deformation parameter, defined as a continuum extension of the Rényi's index (or Tsallis's α), with clear geometrical interpretation, i.e. the scalar curvature of the manifold. Concretely, let's consider the Rényi entropy with parameter $\gamma \geq -1$, given by

$$H_\gamma = -\frac{1}{\gamma} \log \sum_{\mathbf{x}} p(\mathbf{x})^{1+\gamma}. \quad (\text{S1.3})$$

This definition adopts the shifted indexing convention introduced in Ref. [43], thereby referring to $\gamma = n - 1$ as the order of Rényi's entropy, with $n \geq 0$ corresponding to the order in the standard definition. Rényi entropy recovers the standard Shannon entropy at the limit $\gamma \rightarrow 0$. The maximisation of the Rényi entropy can be performed by extremisation of the Lagrangian:

$$\mathcal{L} = -\frac{1}{\gamma} \log \sum_{\mathbf{x}} p(\mathbf{x})^{1+\gamma} + \theta_0 \left(\sum_{\mathbf{x}} p(\mathbf{x}) - 1 \right) + \theta_0 \gamma \beta \sum_{i=1}^L \theta_i \left(\sum_{\mathbf{x}} p(\mathbf{x}) f_i(\mathbf{x}) - c_i \right), \quad (\text{S1.4})$$

which also consider constraints $\sum_{\mathbf{x}} p(\mathbf{x}) = 1$ and $\sum_{\mathbf{x}} p(\mathbf{x}) f_i(\mathbf{x}) = c_i$ with $i = 1, \dots, L$, whereas the first ensures $p(\mathbf{x})$ to be a probability mass function and the second fixes the average of $f_i(\mathbf{x})$ on a desired value c_i . Note that the coefficient β is introduced to keep γ dimensionless, corresponding to the inverse temperature in statistical physics. This results into the maximum entropy condition

$$0 = \frac{\delta \mathcal{L}}{\delta p(\mathbf{x})} = -\frac{1}{\gamma} \frac{(1+\gamma)p(\mathbf{x})^\gamma}{\sum_{\mathbf{x}} p(\mathbf{x})^{1+\gamma}} + \theta_0 + \theta_0 \gamma \beta \sum_a \theta_a f_a(\mathbf{x}). \quad (\text{S1.5})$$

The family of probability distributions meeting the above condition is known as the *deformed exponential family*, which is given by

$$p_\gamma(\mathbf{x}) = \exp(-\varphi_\gamma) \left[1 + \gamma \beta \sum_a \theta_a f_a(\mathbf{x}) \right]_+^{1/\gamma} \quad (\text{S1.6})$$

where φ_γ is a normalising constant

$$\varphi_\gamma = \log \sum_{\mathbf{x}} \left[1 + \gamma \beta \sum_a \theta_a f_a(\mathbf{x}) \right]_+^{1/\gamma}. \quad (\text{S1.7})$$

Above, we use the square bracket $[\cdot]_+$ operator to sets negative values to zero, so that $[x]_+ = \max\{0, x\}$. In the next sections, to solve the steepest descent step of mean field calculations, we will assume that the content of the $[\cdot]_+$ operator is always possible, so differentiation is always positive. This assumption is reasonable under an adequate normalisation of γ .

Importantly, Rényi's entropy is closely related to Tsallis' entropy

$$H_\gamma^{(\text{Ts})} = -\frac{1}{\gamma} \left(1 - \sum_{\mathbf{x}} p(\mathbf{x})^{1+\gamma} \right). \quad (\text{S1.8})$$

It can be shown that the Tsallis and Rényi's entropies can be deformed into one another by a monotonically increasing function. This fact brings both divergences, from the geometrical perspective, to the same equivalence class generating the same geometry, see Ref. [42]. In particular, by maximising Tsallis entropy one recovers the same deformed exponential family, p_γ using $q = 1 - \gamma$ [44].

Supplementary Note 2: Glauber rule

Glauber dynamics is a Markov Chain Monte Carlo algorithm that is popular for simulating neural activity according to Hopfield networks and Ising models. In this method, one samples the activity of each neuron conditioned on the activity of other neurons according to the following conditional distribution:

$$p_\gamma(x_k|\mathbf{x}_{\setminus k}) = \frac{p_\gamma(x_k, \mathbf{x}_{\setminus k})}{p_\gamma(\mathbf{x}_{\setminus k})} = \frac{p_\gamma(x_k, \mathbf{x}_{\setminus k})}{p_\gamma(x_k, \mathbf{x}_{\setminus k}) + p_\gamma(-x_k, \mathbf{x}_{\setminus k})} = \frac{1}{1 + \frac{p_\gamma(-x_k, \mathbf{x}_{\setminus k})}{p_\gamma(x_k, \mathbf{x}_{\setminus k})}}, \quad (\text{S2.1})$$

where $\mathbf{x}_{\setminus k}$ denotes the state of all neurons except the k -th one. This sampling procedure is carried out for all neurons in an iterative manner.

Let us construct Glauber dynamics for a curved neural network. The deformed exponential family distribution states that the distribution of \mathbf{x} is given by

$$p_\gamma(\mathbf{x}) = \exp(-\varphi_\gamma) [1 - \gamma\beta E(\mathbf{x})]_+^{1/\gamma}, \quad (\text{S2.2})$$

where the energy function $E(\mathbf{x})$ is given by

$$E(\mathbf{x}) = -\sum_i H_i x_i - \frac{1}{2N} \sum_{i,j} J_{ij} x_i x_j. \quad (\text{S2.3})$$

The deformed exponential family distribution can be rewritten as

$$p_\gamma(-x_k, \mathbf{x}_{\setminus k}) = \exp(-\varphi) [1 - \gamma\beta (E(\mathbf{x}) + 2x_k h_k)]_+^{1/\gamma}, \quad (\text{S2.4})$$

with $h_k = H_k + \frac{1}{2N} \sum_j J_{kj} x_j$. Under the assumption of $1 - \gamma\beta E(\mathbf{x}) > 0$ (and the same for the state resulting from flipping the k -th spin), a direct derivation shows that

$$\begin{aligned} p_\gamma(x_k|\mathbf{x}_{\setminus k}) &= \left(1 + \left(\frac{1 - \gamma\beta (E(\mathbf{x}) + 2x_k h_k)}{1 - \gamma\beta E(\mathbf{x})} \right)^{1/\gamma} \right)^{-1} \\ &= \left(1 + (1 - \gamma 2\beta' x_k h_k)^{1/\gamma} \right)^{-1} \\ &= (1 + \exp_\gamma(-2\beta' x_k h_k))^{-1} \end{aligned} \quad (\text{S2.5})$$

$$\beta' = \frac{\beta}{1 - \gamma\beta E(\mathbf{x})}. \quad (\text{S2.6})$$

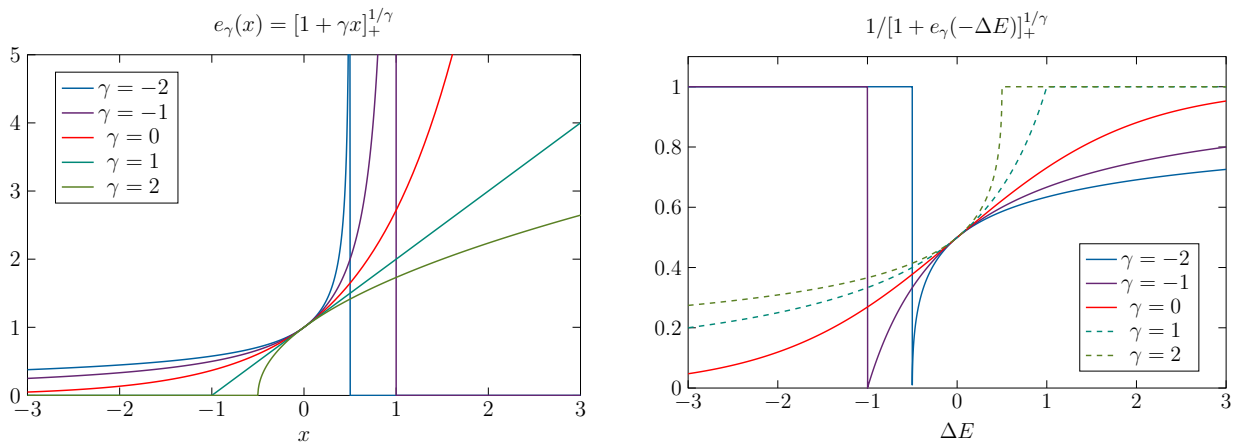


FIG. S1. (Left) The deformed exponential functions, $e_\gamma(x) = [1 + \gamma x]_+^{1/\gamma}$. (Right) The activation function of a neuron as a function of input ΔE .

where $\exp_\gamma(\cdot)$ stands for the deformed exponential. Note that these equations recover the classical Glauber rule for Ising models at $\gamma = 0$. Supplementary Fig. 1 shows the deformed exponential function and the activation function $p_\gamma(x_k = 1|\mathbf{x}_{\setminus k})$ as a function of input $\Delta E = 2\beta' h_k$, representing the deformed nonlinearity of a neuron. Note that to have a smooth activation function, the input must satisfy $1 + \gamma\Delta E > 0$, resulting in $\Delta E > -1/\gamma$ if $\gamma > 0$ and $\Delta E < -1/\gamma$ if $\gamma < 0$. For implementing the sampling strategy, the selection of neurons can be sequential, using random permutations, or using probabilistic methods (according to non-zero probabilities assigned to each neuron).

In the case of large systems in which $E(\mathbf{x})$ extensive, then a normalisation of the curvature parameter in the form $\gamma' = \frac{\gamma}{N}$ is required. This makes the value of $\gamma x_k h_k$ to tend to zero as $N \rightarrow \infty$. In this case, calculating the limit of $\exp_\gamma(-2\beta' x_k h_k)$ as $\gamma \rightarrow 0$, one finds that

$$p_\gamma(x_k|\mathbf{x}_{\setminus k}) = (1 + \exp(-2\beta' x_k h_k))^{-1} = \frac{\exp(\beta' x_k h_k)}{\cosh(\beta' h_k)}, \quad (\text{S2.7})$$

with effective temperature β' given by

$$\beta' = \frac{\beta}{1 - \gamma' \frac{1}{N} \beta E(\mathbf{x})} \quad (\text{S2.8})$$

and

$$\tilde{m}_k(\mathbf{x}) = \tanh(\beta' h_k). \quad (\text{S2.9})$$

Supplementary Note 3: The mean-field theory of curved neural network

1. Derivation of general mean-field solution

In this section we study a curved neural network composed of N neurons that stores M patterns $\boldsymbol{\xi}^a = (\xi_1^a, \dots, \xi_N^a)$, as described by the deformed exponential family distribution given by

$$p_\gamma(\mathbf{x}) = \exp(-\varphi_\gamma) \left[1 + \gamma\beta \left(H \sum_{a,i} \xi_i^a x_i + \frac{J}{N} \sum_{a,i < j} x_i \xi_i^a \xi_j^a x_j \right) \right]_+^{1/\gamma}, \quad (\text{S3.1})$$

where φ_γ is the normalising potential and γ is the deformation parameter. In the following sections we assume that parameters are scaled so to that the content of the brackets $[]_+$ is always positive, to avoid non-differentiable values.

We start the analysis by computing the value of $\exp(\varphi)$ in the large N limit, which can be done employing a delta integral substituting the value of $\frac{1}{N} \sum_i x_i$:

$$\begin{aligned} \exp(\varphi_\gamma) &= \sum_{\mathbf{x}} \left[1 + \gamma\beta \left(H \sum_{a,i} \xi_i^a x_i + \frac{J}{N} \sum_{a,i < j} x_i \xi_i^a \xi_j^a x_j \right) \right]_+^{1/\gamma} \\ &= \sum_{\mathbf{x}} \exp \left(\frac{1}{\gamma} \log \left(1 + \gamma\beta \left(H \sum_{a,i} \xi_i^a x_i + \sum_a \frac{J}{2N} \left(\left(\sum_i \xi_i^a x_i \right)^2 - N \right) \right) \right) \right), \end{aligned} \quad (\text{S3.2})$$

where the second equality uses $(\sum_i z_i)^2 - N = 2 \sum_{i < j} z_i z_j$. Additionally, by replacing $\frac{1}{N} \sum_i \xi_i^a x_i$ by a Dirac delta function under an integral, and then using the delta function's integral form $\delta(x - a) = \frac{1}{2\pi} \int_{-\infty}^{\infty} e^{i\zeta(x-a)} d\zeta$, the expression above can be re-written as

$$\begin{aligned} \exp(\varphi_\gamma) &= \sum_{\mathbf{x}} \int d\mathbf{m} \prod_a \delta \left(m_a - \frac{1}{N} \sum_i \xi_i^a x_i \right) \exp \left(\frac{1}{\gamma} \log \left(1 + \gamma N \beta \sum_a \left(H m_a + \frac{J}{2} \left(m_a^2 - \frac{1}{N} \right) \right) \right) \right) \\ &= \frac{1}{(2\pi)^M} \int d\mathbf{m} d\hat{\mathbf{m}} \sum_{\mathbf{x}} \exp \left(\frac{1}{\gamma} \log \left(1 + \gamma N \beta \sum_a \left(H m_a + \frac{J}{2} \left(m_a^2 - \frac{1}{N} \right) \right) \right) - \sum_a i \hat{m}_a \left(m_a - \frac{1}{N} \sum_i \xi_i^a x_i \right) \right). \end{aligned} \quad (\text{S3.3})$$

Let us now introduce a scaling rule for the deformation parameter γ given by

$$\gamma = \frac{\gamma'}{\beta N}, \quad (\text{S3.4})$$

where γ' is a constant independent of N , which is motivated by subsequent results for the mean-field solution that suggest this relationship between γ and N in order to maintain scale-invariant properties. Then, the potential φ_γ can be expressed in terms of γ' as

$$\begin{aligned} \exp(\varphi_\gamma) &= \frac{1}{(2\pi)^M} \int d\mathbf{m} d\hat{\mathbf{m}} \exp \left(\frac{N\beta}{\gamma'} \log \left(1 + \gamma' \sum_a \left(H m_a + \frac{J}{2} \left(m_a^2 - \frac{1}{N} \right) \right) \right) \right. \\ &\quad \left. - \sum_a i \hat{m}_a m_a + \sum_i \log \left(2 \cosh \left(\frac{1}{N} \sum_a \xi_i^a i \hat{m}_a \right) \right) \right). \end{aligned} \quad (\text{S3.5})$$

Under this condition, the exponent in the equation above goes to infinity as $N \rightarrow \infty$. In this limit, the integral can be evaluated by the method of the steepest descent (a.k.a. the saddle-point method). By differentiating the exponent by \hat{m}_a , we find the saddle point must satisfy

$$m_a = \frac{1}{N} \sum_i \xi_i^a \tanh \left(\frac{1}{N} \sum_b \xi_i^b i \hat{m}_b \right). \quad (\text{S3.6})$$

Similarly, differentiating by m_a yields

$$i \hat{m}_a = \beta' N (H + J m_a), \quad (\text{S3.7})$$

where we introduced the effective inverse temperature β' :

$$\beta' = \frac{\beta}{1 + \gamma' \sum_b (H m_b + \frac{J}{2} m_b^2)}. \quad (\text{S3.8})$$

From these equations, we find the mean field solution in the limit of large N :

$$m_a = \frac{1}{N} \sum_i \xi_i^a \tanh \left(\beta' \sum_b \xi_i^b (H + J m_b) \right), \quad (\text{S3.9})$$

which recovers the classical mean field solution at $\gamma' = 0$. This solution confirms that γ has to be scaled by the system size to maintain the scale-invariant properties.

The normalising potential in the large N limit is obtained as

$$\varphi_\gamma = \frac{\beta N}{\gamma'} \log \frac{\beta'}{\beta} - \sum_a m_a \beta' N (H + J m_a) + \sum_i \log \left(2 \cosh \left(\beta' \sum_a \xi_i^a (H + J m_a) \right) \right). \quad (\text{S3.10})$$

2. A single pattern: explosive phase transitions

When embedded memory contains only a single pattern ($M = 1$), the equations above result in

$$\varphi_\gamma = \frac{\beta N}{\gamma'} \log \frac{\beta'}{\beta} - N \beta' (H + J m) m + N \log (2 \cosh (\beta' (H + J m))), \quad (\text{S3.11})$$

with

$$m = \tanh (\beta' (H + J m)), \quad (\text{S3.12})$$

$$\beta' = \frac{\beta}{1 + \gamma' (H m + \frac{J}{2} m^2)}. \quad (\text{S3.13})$$

Under the limit of small γ given by the scaling (S3.4), the derivative of the normalisation potential φ_γ w.r.t. H yields the corresponding expected value, similarly to the exponential family distribution. Then, $\gamma' = 0$ yields the classical result. This can be verified by

$$\begin{aligned} \frac{\partial \varphi_\gamma}{\partial H} &= -\frac{\beta N}{\gamma'} \frac{\partial \beta'}{\partial H} - N \beta' (H + J m) \frac{\partial m}{\partial H} - N \frac{\partial \beta' (H + J m)}{\partial H} m + N \frac{\partial \beta' (H + J m)}{\partial H} m \\ &= -\frac{\beta N}{\gamma'} \frac{\partial \beta'}{\partial H} - N \beta' (H + J m) \frac{\partial m}{\partial H}, \end{aligned} \quad (\text{S3.14})$$

where

$$\frac{\partial \beta'}{\partial H} = \frac{-\beta \gamma' (m + \frac{\partial m}{\partial H} (H + J m))}{(1 + \gamma' (H m + \frac{J}{2} m^2))^2} = -\beta^{-1} \beta'^2 \gamma' (m + \frac{\partial m}{\partial H} (H + J m)), \quad (\text{S3.15})$$

resulting in

$$\frac{\partial \varphi_\gamma}{\partial H} = N \beta' (m + \frac{\partial m}{\partial H} (H + J m)) - N \beta' (H + J m) \frac{\partial m}{\partial H} \quad (\text{S3.16})$$

$$= N \beta' m. \quad (\text{S3.17})$$

The result recovers the classical relation, $\frac{\partial \varphi_\gamma}{\partial H} = \beta N m$ for the case $\gamma' = 0$.

a. Behaviour at criticality

Now, we compute the critical exponents of the mean-field parameter for $H = 0$. In the thermodynamic limit with $\gamma = \gamma' / (\beta N)$, one finds that

$$m = \tanh \left(\frac{\beta J m}{1 + \gamma' \frac{J}{2} m^2} \right). \quad (\text{S3.18})$$

Since $\tanh\left(\frac{am}{1+bm}\right) = am - (a^3/3 + ab)m^3 + O(m^4)$, by expanding the r.h.s. around $m = 0$ up to the third order one can find that

$$m = \beta J m - \frac{1}{6}(\beta J) (2(\beta J)^2 + 3J\gamma') m^3 + \mathcal{O}(m^4), \quad (\text{S3.19})$$

which yields a trivial solution at $m = 0$ and two non-trivial solutions given by

$$m_{\pm} = \pm \sqrt{\frac{\beta J - 1}{\frac{1}{6}\beta J (2(\beta J)^2 + 3J\gamma')}}. \quad (\text{S3.20})$$

which yields a mean-field universality class critical exponent ‘beta’ (not to be confused with the inverse temperature) of $\frac{1}{2}$.

The magnetic susceptibility, $\chi := \frac{\partial m}{\partial H}$, of the deformed Ising model can be calculated using (S3.13). Hence, we have

$$\frac{\partial m}{\partial H} = (1 - m^2) \left(\beta' \left(1 + J \frac{\partial m}{\partial H} \right) + \frac{\partial \beta'}{\partial H} (H + Jm) \right). \quad (\text{S3.21})$$

Using (S3.15), we obtain

$$\begin{aligned} \frac{\partial m}{\partial H} &= (1 - m^2) \left(\beta' \left(1 + J \frac{\partial m}{\partial H} \right) - \beta^{-1} \beta' \gamma' \left(m + \frac{\partial m}{\partial H} (H + Jm) \right) (H + Jm) \right) \\ &= (1 - m^2) \beta' \left(1 + J \frac{\partial m}{\partial H} - \frac{\beta'}{\beta} \gamma' \left(m + \frac{\partial m}{\partial H} (H + Jm) \right) (H + Jm) \right) \\ &= (1 - m^2) \beta' \left(1 - \frac{\beta'}{\beta} \gamma' m (H + Jm) + \frac{\partial m}{\partial H} \left(J - \frac{\beta'}{\beta} \gamma' (H + Jm)^2 \right) \right). \end{aligned} \quad (\text{S3.22})$$

Then, we obtain

$$\frac{\partial m}{\partial H} = \frac{(1 - m^2) \beta' \left(1 - \frac{\beta'}{\beta} \gamma' m (H + Jm) \right)}{1 - (1 - m^2) \beta' \left(J - \frac{\beta'}{\beta} \gamma' (H + Jm)^2 \right)}. \quad (\text{S3.23})$$

The susceptibility $\frac{dm}{dH}$ at $m = 0$ is

$$\frac{\partial m}{\partial H} = \frac{\beta}{1 - \beta \left(J - \frac{\beta'}{\beta} \gamma' H^2 \right)} \quad (\text{S3.24})$$

$$= \frac{-\beta \beta_c}{\beta - \beta_c}, \quad (\text{S3.25})$$

where the critical inverse temperature is given by $\beta_c = 1/(J - \frac{\beta'}{\beta} \gamma' H^2)$. Thus the susceptibility results in the universality class ‘gamma’ exponent of 1 (not to be confused with the deformation parameter) near the critical temperature. At $H = 0$, $\beta_c = 1/J$.

At $\gamma' = 0$, we recover

$$\frac{\partial m}{\partial H} = \frac{(1 - m^2) \beta}{1 - (1 - m^2) \beta J}. \quad (\text{S3.26})$$

3. Two correlated patterns

Here we study an exemplary case in which two patterns are embedded in the deformed associative network, with $\langle \xi_i^1 \xi_i^2 \rangle = C$. We seek solutions for (11) which can be further simplified for the case of two correlated patterns. Let us focus on its cosh term, i.e. $\cosh(\xi_i^1 \theta_1 + \xi_i^2 \theta_2)$ where $\theta_a = \beta' (H + Jm_a)$ and $a = 1, 2$. Noting that $(\xi_i^a)^2 = 1$, we can define $P_{\pm} = \frac{1}{2}(1 + \xi_i^1 \xi_i^2)$, these act as projection operators ($P_{\pm}^2 = P_{\pm}$ and $P_{+} P_{-} = 0$). It can then be found that,

$$\begin{aligned} \xi_i^1 \theta_1 + \xi_i^2 \theta_2 &= (P_{+} + P_{-})(\xi_i^1 \theta_1 + \xi_i^2 \theta_2) \\ &= \frac{\xi_i^1 + \xi_i^2}{2} \lambda_{+} + \frac{\xi_i^1 - \xi_i^2}{2} \lambda_{-}, \end{aligned} \quad (\text{S3.27})$$

where $\lambda_{\pm} := \theta_1 \pm \theta_2$. By using the properties of ξ_i^a and the projection operators, one can express (S3.27) in terms of P_{\pm} as

$$\sqrt{\left(\frac{\xi_i^1 + \xi_i^2}{2}\lambda_+ + \frac{\xi_i^1 - \xi_i^2}{2}\lambda_-\right)^2} = \sqrt{P_+\lambda_+^2 + P_-\lambda_-^2} = P_+\lambda_+ + P_-\lambda_- \quad (\text{S3.28})$$

Note that one can expand of a function of argument $P_+\lambda_+ + P_-\lambda_-$ as

$$(P_+\lambda_+ + P_-\lambda_-)^n = \sum_{k=0}^n \binom{n}{k} (P_+\lambda_+)^k (P_-\lambda_-)^{n-k} = (P_+\lambda_+)^n + (P_-\lambda_-)^n, \quad (\text{S3.29})$$

since any cross term involving $P_{\pm}P_{\mp}$ vanish. This allows us to express the last term in (11) as

$$\log(2 \cosh(\xi_i^1 \theta_1 + \xi_i^2 \theta_2)) = P_+ \log(2 \cosh(\lambda_+)) + P_- \log(2 \cosh(\lambda_-)). \quad (\text{S3.30})$$

Hence, by replacing terms, one can find that

$$m_1 = \frac{1+C}{2} \tanh(\beta'(2H + Jm_1 + Jm_2)) + \frac{1-C}{2} \tanh(\beta'(Jm_1 - Jm_2)), \quad (\text{S3.31})$$

$$m_2 = \frac{1+C}{2} \tanh(\beta'(2H + Jm_1 + Jm_2)) - \frac{1-C}{2} \tanh(\beta'(Jm_1 - Jm_2)). \quad (\text{S3.32})$$

The normalising potential then becomes

$$\begin{aligned} \varphi_{\gamma} &= \frac{\beta N}{\gamma'} \log \frac{\beta'}{\beta} - \beta' N m_1 (H + Jm_1) - \beta' N m_2 (H + Jm_2) \\ &\quad + \frac{1+C}{2} N \log(2 \cosh(\beta'(2H + Jm_1 + Jm_2))) + \frac{1-C}{2} N \log(2 \cosh(\beta'(Jm_1 - Jm_2))). \end{aligned} \quad (\text{S3.33})$$

Supplementary Note 4: Dynamical mean-field theory

Let us now describe the statistics of temporal trajectories of the system. For this, let's consider the trajectory $\mathbf{x}_{0:T} = (\mathbf{x}_0, \dots, \mathbf{x}_T)$, whose probability can be computed as

$$p_\gamma(\mathbf{x}_{0:T}) = \prod_t p_\gamma(\mathbf{x}_t | \mathbf{x}_{t-1}), \quad (\text{S4.1})$$

where the probability of the transition between \mathbf{x}_{t-1} and \mathbf{x}_t can be expressed as

$$p_\gamma(\mathbf{x}_t | \mathbf{x}_{t-1}) = \sum_i p_\gamma(x_{i,t} | \mathbf{x}_{t-1}) \prod_{j \neq i} \delta(x_{j,t}, x_{j,t-1}), \quad (\text{S4.2})$$

where the individual transitions can be expressed as

$$p_\gamma(x_{i,t} | \mathbf{x}_{t-1}) = \left(1 + \exp_\gamma \left(-2\beta'_t x_{i,t} h_{i,t} \right) \right)^{-1}, \quad (\text{S4.3})$$

$$h_{i,t} = \sum_a \left(\xi_i^a H^a + \sum_a \frac{1}{2N} \sum_j \xi_i^a \xi_j^a x_{j,t-1} \right), \quad (\text{S4.4})$$

$$\beta'_t = \frac{\beta}{1 + \gamma' \left(\frac{1}{N} \sum_i x_{i,t-1} \sum_a \left(\xi_i^a H^a + \frac{1}{2N} \sum_j \xi_i^a \xi_j^a x_{j,t-1} \right) \right)}, \quad (\text{S4.5})$$

and $\delta(x, y)$ is the Kronecker delta. As before, the above derivation assumes that the content of the $[]_+$ operator in the definition of the deformed exponential family is non-negative.

Under the Glauber dynamics described in the previous subsection, the statistics of trajectories of the system take the following form:

$$\begin{aligned} p_\gamma(\mathbf{x}_t | \mathbf{x}_{t-1}) &= \frac{1}{N} \sum_i p_\gamma(x_{i,t} | \mathbf{x}_{t-1}) \prod_{j \neq i} \delta(x_{j,t}, x_{j,t-1}) \\ &= \frac{1}{N(2\pi)^{N-1}} \sum_i \int_0^{2\pi} d\phi_t \exp \left(\beta'_t x_{i,t} h_{i,t} - \log(2 \cosh(\beta'_t h_{i,t})) + \sum_{j \neq i} i\phi_{j,t}(x_{j,t} - x_{j,t-1}) \right). \end{aligned} \quad (\text{S4.6})$$

The terms in the summation can be regarded as an average of vectors $\boldsymbol{\tau}_t$ such that $\tau_{j,t}^i = \delta[i, j]$ for $j = 1, \dots, N$ (i.e., a one-hot encoding of j). Using this, the probability of the trajectory $\mathbf{x}_{0:t}$ can be rewritten as

$$\begin{aligned} p_\gamma(\mathbf{x}_{0:t}) &= \frac{1}{N^t (2\pi)^{Nt}} \sum_{\boldsymbol{\tau}} \int_0^{2\pi} d\phi \exp \left(\sum_{i,t} \left((\beta'_t x_{i,t} h_{i,t} - \log(2 \cosh(\beta'_t h_{i,t}))) \tau_{i,t}^i \right. \right. \\ &\quad \left. \left. - \sum_{j \neq i,t} i\phi_{j,t}(x_{j,t} - x_{j,t-1})(1 - \tau_{j,t}^i) \right) \right). \end{aligned} \quad (\text{S4.7})$$

In equilibrium systems, the partition function retrieves their statistical moments. A nonequilibrium equivalent function is a generating functional or dynamical partition function [57]. Let us now define the generating functional

$$Z(\mathbf{g}) = \sum_{\mathbf{x}} \exp \left(\sum_{i,t} g_{i,t} x_{i,t} \right) p_\gamma(\mathbf{x}_{0:t}), \quad (\text{S4.8})$$

such that the following relationship is satisfied:

$$\frac{dZ(\mathbf{0})}{dg_{i,t}} = \langle x_{i,t} \rangle. \quad (\text{S4.9})$$

Then, one can find an analytical expression for the functional by introducing delta integrals of the following form:

$$\begin{aligned}
Z(\mathbf{g}) &= \frac{1}{(N+M)t(2\pi)^{Nt}} \sum_{\mathbf{x}} \sum_{\boldsymbol{\tau}} \int_0^{2\pi} d\phi \exp \left(\sum_{i,t} \left(\left((g_{i,t} + \beta'_t h_{i,t}) x_{i,t} - \sum_{i,t} \log(2 \cosh(\beta'_t h_{i,t})) \right) \tau_{i,t}^i \right. \right. \\
&\quad \left. \left. - \sum_{j \neq i,t} i\phi_{j,t}(x_{j,t} - x_{j,t-1})(1 - \tau_{j,t}^i) \right) \right) \\
&= \frac{1}{Nt(2\pi)^{Nt}} \sum_{\mathbf{x}} \sum_{\boldsymbol{\tau}} \int_0^{2\pi} d\phi \exp \left(\sum_{i,t} \left(\left((g_{i,t} + \tilde{\beta}'_t \tilde{h}_{i,t}) x_{i,t} - \sum_{i,t} \log(2 \cosh(\tilde{\beta}'_t \tilde{h}_{i,t})) \right) \tau_{i,t}^i \right. \right. \\
&\quad \left. \left. - \sum_{j \neq i,t} i\phi_{j,t}(x_{j,t} - x_{j,t-1})(1 - \tau_{j,t}^i) - \sum_{a,t} i\hat{m}_{a,t} \left(m_{a,t} - \frac{1}{N} \sum_i \xi_i^a x_{i,t} \right) \right) \right) \\
&= \frac{1}{Nt(2\pi)^{Nt}} \sum_{\boldsymbol{\tau}} \int_0^{2\pi} d\phi \prod_i \sum_{\mathbf{x}_i} \exp \left(\sum_{i,t} \left(\left(x_{i,t} \left(g_{i,t} + \tilde{\beta}'_t \tilde{h}_{i,t} + \frac{1}{N} \sum_b i\hat{m}_{b,t} \xi_i^b \right) - \sum_{i,t} \log(2 \cosh(\tilde{\beta}'_t \tilde{h}_{i,t})) \right) \tau_{i,t}^i \right. \right. \\
&\quad \left. \left. - \sum_{j \neq i,t} i\phi_{j,t}(x_{j,t} - x_{j,t-1})(1 - \tau_{j,t}^i) - \sum_{a,t} i\hat{m}_{a,t} m_{a,t} \right) \right), \tag{S4.10}
\end{aligned}$$

with

$$\tilde{h}_{i,t} = \sum_a \xi_i^a (H^a + m_{a,t-1}), \tag{S4.11}$$

$$\tilde{\beta}'_t = \frac{\beta}{1 + \gamma' \sum_a (H^a m_{a,t-1} + \frac{1}{2} m_{a,t-1}^2)}. \tag{S4.12}$$

One can solve the mean-field equations via steepest descent, obtaining

$$m_{a,t}(\mathbf{g}) = m_{a,t-1} \left(1 - \frac{1}{N} \right) + \frac{1}{N^2} \sum_i \xi_i^a \tanh \left(g_{i,t} + \tilde{\beta}'_t \tilde{h}_{i,t} + \frac{1}{N} \sum_b \xi_i^b i\hat{m}_{b,t} \right), \tag{S4.13}$$

$$i\hat{m}_{a,t} = \tilde{\beta}'_t \sum_i \xi_i^a \left(\tanh \left(g_{i,t+1} + \tilde{\beta}'_{t+1} \tilde{h}_{i,t+1} + \frac{1}{N} \sum_b \xi_i^b i\hat{m}_{b,t} \right) - \tanh(\tilde{\beta}'_t \tilde{h}_{i,t+1}) \right). \tag{S4.14}$$

The system is solved at $\mathbf{g} = \mathbf{0}$ for

$$m_{a,t} = m_{a,t-1} \left(1 - \frac{1}{N} \right) + \frac{1}{N^2} \sum_i \xi_i^a \tanh \left(\tilde{\beta}'_t \tilde{h}_{i,t} \right). \tag{S4.15}$$

Under large N and for an adequate time re-scaling, this leads to the following differential equation:

$$\dot{m}_a = -m_a + \frac{1}{N} \sum_i \xi_i^a \tanh \left(\beta' \sum_b \xi_i^b (H^b + m_b) \right), \tag{S4.16}$$

$$\beta' = \frac{\beta}{1 + \gamma' \sum_a (H^a m_a + \frac{1}{2} m_a^2)}. \tag{S4.17}$$

Supplementary Note 5: Replica analysis near saturation

Here we analyse a curved neural network with an extensive number of patterns, $M = \alpha N$ in (5). The model involves integrals over a large number of variables, making the steepest descent method inapplicable. Instead, we adopt the approach reported in Ref. [60], and average the free energy over the distribution of patterns using the replica trick.

For $Z = \exp(\varphi_\gamma)$, the replica trick is applied as follows:

$$\langle\langle \varphi_\gamma \rangle\rangle = \langle\langle \log Z \rangle\rangle = \lim_{n \rightarrow 0} \frac{1}{n} (\langle\langle Z^n \rangle\rangle - 1), \quad (\text{S5.1})$$

which can be equivalently written as

$$\langle\langle \log Z \rangle\rangle = \lim_{n \rightarrow 0} \frac{1}{n} \log \langle\langle Z^n \rangle\rangle, \quad (\text{S5.2})$$

with $\langle\langle f(\mathbf{x}) \rangle\rangle = 2^{-MN} \sum_{\boldsymbol{\xi}} f(\mathbf{x})$ being the configurational average over different combinations of the systems parameters.

1. General derivation

To calculate the encoding of patterns, we introduce $\{\boldsymbol{\xi}_a\}$ with $a = 1, \dots, M$ where the first l patterns are given — called ‘nominated’ patterns — and we average over the $M - l$ rest. Again, assuming as in Section 3 that the content of the $[]_+$ is positive, we calculate

$$\langle\langle Z^n \rangle\rangle = \frac{1}{2^{N(M-l)}} \sum_{\boldsymbol{\xi}^{a>l}} \sum_{\mathbf{x}} \exp \left(\frac{1}{\gamma} \sum_u \log \left(1 + \gamma \beta \left(\sum_b H_b \frac{1}{N} \sum_i x_i^u \xi_i^b + \frac{J}{N} \sum_a \sum_{i<j} x_i^u \xi_i^a \xi_j^a x_j^u \right) \right) \right). \quad (\text{S5.3})$$

We want to compute the configurational average of a network with M memories with $N, M \rightarrow \infty$ and $M/N = \alpha$, introducing a pair of delta integrals

$$\begin{aligned} \langle\langle Z^n \rangle\rangle &= \frac{1}{(2\pi)^{(l+1)n}} \int d\mathbf{m} d\hat{\mathbf{m}} d\boldsymbol{\mu} d\hat{\boldsymbol{\mu}} \sum_{\boldsymbol{\xi}^{a>l}} \sum_{\mathbf{x}} \exp \left(\frac{1}{\gamma} \sum_u \log \left(1 + \gamma \beta \left(\sum_b \left(N H_b m_b^u + \frac{JN}{2} (m_b^u)^2 \right) + J\mu_u - N \frac{J\alpha}{2} \right) \right) \right. \\ &\quad \left. - \sum_{u,b} i \hat{m}_b^u \left(m_b^u - \frac{1}{N} \sum_i x_i^u \xi_i^b \right) - \sum_u i \hat{\mu}_u \left(\mu_u - \frac{1}{2} \sum_{a>l} \left(\frac{1}{\sqrt{N}} \sum_i x_i^u \xi_i^a \right)^2 \right) \right), \end{aligned} \quad (\text{S5.4})$$

leading to

$$\begin{aligned} \langle\langle Z^n \rangle\rangle &= \frac{1}{(2\pi)^{(l+1)n}} \int d\mathbf{m} d\hat{\mathbf{m}} d\boldsymbol{\mu} d\hat{\boldsymbol{\mu}} \sum_{\mathbf{x}} \exp \left(\frac{1}{\gamma} \sum_u \log \left(1 + \gamma \beta \left(\sum_b \left(N H_b m_b^u + \frac{JN}{2} (m_b^u)^2 \right) + J\mu_u - N \frac{J\alpha}{2} \right) \right) \right. \\ &\quad \left. - \sum_{u,b} i \hat{m}_b^u \left(m_b^u - \frac{1}{N} \sum_i x_i^u \xi_i^b \right) - \sum_u i \hat{\mu}_u \mu_u + \log \left(\frac{1}{2^{N(M-l)}} \sum_{\boldsymbol{\xi}^{a>l}} \exp \left(\sum_u \frac{1}{2} \sum_{a>l} \left(\sqrt{\frac{i \hat{\mu}_u}{N}} \sum_i x_i^u \xi_i^a \right)^2 \right) \right) \right). \end{aligned} \quad (\text{S5.5})$$

We can integrate over disorder by factorising over patterns a and introducing a Gaussian integral

$$\begin{aligned}
\frac{1}{2^{N(M-l)}} \sum_{\xi^{a>l}} \exp \left(\sum_{a>l} \sum_u \left(\frac{1}{2} \sqrt{\frac{\hat{\mu}_u}{N}} \sum_i x_i^u \xi_i^a \right)^2 \right) &= \frac{1}{2^{N(M-l)}} \prod_{a>l} \sum_{\xi^a} \exp \left(\sum_u \frac{1}{2} \left(\sqrt{\frac{\hat{\mu}_u}{N}} \sum_i x_i^u \xi_i^a \right)^2 \right) \\
&= \prod_{a>l} \frac{1}{2^{N(M-l)}} \sum_{\xi^a} \int D\mathbf{z} \exp \left(\sum_u z_u \sqrt{\frac{\hat{\mu}_u}{N}} \sum_i x_i^u \xi_i^a \right) \\
&= \frac{1}{2^{N(M-l)}} \left(\int D\mathbf{z} \exp \left(\sum_i \log 2 \cosh \left(\sum_u \sqrt{\frac{\hat{\mu}_u}{N}} z_u x_i^u \right) \right) \right)^{M-l} \\
&= \left(\int D\mathbf{z} \exp \left(\frac{1}{2} \sum_{u,v} z_u z_v \sqrt{\hat{\mu}_u \hat{\mu}_v} \frac{1}{N} \sum_i x_i^u x_i^v \right) \right)^{M-l}, \quad (\text{S5.6})
\end{aligned}$$

where the cosh term was expanded assuming a large N . By introducing an additional delta integral for order parameters q_{uv} (assuming $q_{uu} = 1$) and applying exp log, one can re-express the last term (assuming $M - l \approx N\alpha$ near saturation) as

$$\begin{aligned}
&\exp \left(N\alpha \log \int D\mathbf{z} \exp \left(\frac{1}{2} \sum_{u,v} z_u z_v \sqrt{\hat{\mu}_u \hat{\mu}_v} \frac{1}{N} \sum_i x_i^u x_i^v \right) \right) \\
&= \frac{1}{(2\pi)^{\frac{n(n-1)}{2}}} \int d\mathbf{q} d\hat{\mathbf{q}} \exp \left(N\alpha \log \int D\mathbf{z} \exp \left(\frac{1}{2} \sum_{u,v} z_u z_v \sqrt{\hat{\mu}_u \hat{\mu}_v} q_{uv} \right) - \sum_{u<v} i\hat{q}_{uv} \left(q_{uv} - \frac{1}{N} \sum_i x_i^u x_i^v \right) \right) \\
&= \frac{1}{(2\pi)^{\frac{n(n-1)}{2}}} \int d\mathbf{q} d\hat{\mathbf{q}} \exp \left(-\frac{1}{2} N\alpha \log \det \mathbf{\Lambda} - \sum_{u<v} i\hat{q}_{uv} \left(q_{uv} - \frac{1}{N} \sum_i x_i^u x_i^v \right) \right), \quad (\text{S5.7})
\end{aligned}$$

with $\Lambda_{uv} = \delta_{uv} - \sqrt{\hat{\mu}_u \hat{\mu}_v} q_{uv} = \delta_{uv}(1 - i\hat{\mu}_u) - q(1 - \delta_{uv})\sqrt{\hat{\mu}_u \hat{\mu}_v}$. Then, the configurational average can be found to be

$$\begin{aligned}
\langle\langle Z^n \rangle\rangle &= \frac{1}{(2\pi)^{(l+1)n + \frac{n(n-1)}{2}}} \int d\boldsymbol{\pi} \sum_{\mathbf{x}} \exp \left(\frac{1}{\gamma} \sum_u \log \left(1 + \gamma\beta \left(\sum_b \left(NH_b m_b^u + \frac{JN}{2} (m_b^u)^2 \right) + J\mu_u - N\frac{J\alpha}{2} \right) \right) \right. \\
&\quad \left. - \sum_{u,b} i\hat{m}_b^u \left(m_b^u - \frac{1}{N} \sum_i x_i^u \xi_i^b \right) - \sum_u i\hat{\mu}_u \mu_u - \frac{1}{2} N\alpha \log |\mathbf{\Lambda}| - \sum_{u<v} i\hat{q}_{uv} \left(q_{uv} - \frac{1}{N} \sum_i x_i^u x_i^v \right) \right) \\
&= \frac{1}{(2\pi)^{(l+1)n + \frac{n(n-1)}{2}}} \int d\boldsymbol{\pi} \exp \left(\frac{1}{\gamma} \sum_u \log \left(1 + \gamma\beta \left(\sum_b \left(NH_b m_b^u + \frac{JN}{2} (m_b^u)^2 \right) + J\mu_u - N\frac{J\alpha}{2} \right) \right) \right. \\
&\quad \left. - \sum_{u,b} i\hat{m}_b^u m_b^u - \sum_u i\hat{\mu}_u \mu_u - \frac{1}{2} N\alpha \log |\mathbf{\Lambda}| - \sum_{u<v} i\hat{q}_{uv} q_{uv} + \log \sum_{\mathbf{x}} \exp L \right), \quad (\text{S5.8})
\end{aligned}$$

where $d\boldsymbol{\pi} := d\mathbf{m} d\hat{\mathbf{m}} d\boldsymbol{\mu} d\hat{\boldsymbol{\mu}} d\mathbf{q} d\hat{\mathbf{q}}$ has been adopted for readability, with

$$L = \sum_{u,b} i\hat{m}_b^u \frac{1}{N} \sum_i x_i^u \xi_i^b + \sum_{u<v} i\hat{q}_{uv} \frac{1}{N} \sum_i x_i^u x_i^v \quad (\text{S5.9})$$

carrying all remaining x_i dependent terms to be summed. The saddle-node solution is given by

$$\begin{aligned}
i\hat{m}_a^u &= N\beta'_u(H_a + Jm_a^u), \\
i\hat{\mu}_u &= \beta'_u J, \\
m_a^u &= \frac{1}{N} \sum_i \xi_i^a \langle x_i^u \rangle_L := \frac{1}{N} \sum_i \xi_i^a \frac{\sum_{\mathbf{x}} x_i^u \exp L}{\sum_{\mathbf{x}} \exp L}, \\
q_{uv} &= \frac{1}{N} \sum_i \langle x_i^u x_i^v \rangle_L = \frac{1}{N} \sum_i \frac{\sum_{\mathbf{x}} x_i^u x_i^v \exp L}{\sum_{\mathbf{x}} \exp L}, \\
i\hat{q}_{uv} &= N\alpha \sqrt{i\hat{\mu}_u i\hat{\mu}_v} \langle z_u z_v \rangle_* = N\alpha J^2 \beta'_u \beta'_v r_{uv}, \\
\mu_u &= \frac{1}{2} N\alpha \sum_v \sqrt{\frac{\beta'_v}{\beta'_u}} q_{uv} \langle z_u z_v \rangle_* = \frac{1}{2} N\alpha J \sum_v \sqrt{\beta'_u \beta'_v} q_{uv} r_{uv}, \\
\beta'_u &= \frac{\beta}{1 + \gamma N \beta_{\frac{1}{2}} \left(\sum_b (2H_b + Jm_b^u) m_b^u + \alpha J^2 \sum_v \sqrt{\beta'_u \beta'_v} q_{uv} r_{uv} - J\alpha \right)}, \\
r_{uv} &= \frac{1}{J \sqrt{\beta'_u \beta'_v}} \langle z_u z_v \rangle_* := \frac{1}{J \sqrt{\beta'_u \beta'_v}} \frac{\int D\mathbf{z} z_u z_v \exp \left(\frac{1}{2} \sum_{u,v} z_u z_v (\sqrt{\beta'_u \beta'_v} J q_{uv}) \right)}{\int D\mathbf{z} \exp \left(\frac{1}{2} \sum_{u,v} z_u z_v (\sqrt{\beta'_u \beta'_v} J q_{uv}) \right)},
\end{aligned} \tag{S5.10}$$

where the operator $\langle f(\mathbf{x}) \rangle_*$ defined above coincide with regular averages once integration is performed. This results into

$$\begin{aligned}
\log \langle Z^n \rangle &= \frac{1}{\gamma} \sum_u \log \left(1 + \gamma \beta \left(\sum_b \left(N H_b m_b^u + \frac{JN}{2} (m_b^u)^2 \right) + J\mu_u - N \frac{J\alpha}{2} \right) \right) \\
&\quad - \sum_{u,b} N \beta'_u (H_b + Jm_b^u) m_b^u - \sum_u \beta'_u J\mu_u - \frac{1}{2} N\alpha \log |\Lambda| - \sum_{u < v} N\alpha \beta'_u \beta'_v J^2 r_{uv} q_{uv} \\
&\quad + \log \sum_{\mathbf{x}} \exp L
\end{aligned} \tag{S5.11}$$

with L being given (due to (S5.9)) by

$$L = \sum_{u,b} \beta'_u (H_b + Jm_b^u) \sum_i x_i^u \xi_i^b + J^2 \alpha \sum_{u < v} \beta'_u \beta'_v r_{uv} \sum_i x_i^u x_i^v. \tag{S5.12}$$

2. Replica symmetry

The replica symmetry ansatz allows us to simplify order parameters $m_b, q_{u,v}$ (for $u \neq v$) to homogeneous values m, q . Assuming a normalised curvature parameter $\gamma = \frac{\gamma'}{N\beta}$ we obtain

$$\begin{aligned}
\frac{1}{n} \log \langle Z^n \rangle &= \frac{N\beta}{\gamma'} \log \left(1 + \gamma' \left(\sum_b \left(H_b m_b + \frac{J}{2} (m_b)^2 \right) + \frac{J}{N} \mu - \frac{J\alpha}{2} \right) \right) \\
&\quad - \sum_b N \beta'_u (H_b + Jm_b) m_b - \beta' J\mu - \frac{1}{2n} N\alpha \log |\mathbf{I} - \tilde{\mathbf{q}}| \\
&\quad - \frac{1}{2} (n-1) N\alpha \beta'^2 J^2 r q + \frac{1}{n} \log \sum_{\mathbf{x}} \exp L,
\end{aligned} \tag{S5.13}$$

where $J\beta'\mu = \frac{1}{2} N\alpha (J\beta')^2 (R + (n-1)qr)$ with

$$L = \beta' \sum_{u,b} (H_b + Jm_b) \sum_i x_i^u \xi_i^b + \sum_{u < v} \beta'^2 J^2 \alpha r \sum_i x_i^u x_i^v, \tag{S5.14}$$

and obtain

$$\begin{aligned}
\log \sum_{\mathbf{x}} \exp L &= \log \sum_{\mathbf{x}} \exp \left(\sum_{u,b} \beta' (H_b + Jm_b) \sum_i \xi_i^b x_i^u + (\beta' J)^2 \alpha r \sum_i \sum_{u < v} x_i^u x_i^v \right) \\
&= \log \prod_i \sum_{\mathbf{x}_i} \exp \left(\beta' \sum_{u,b} (H_b + Jm_b) \xi_i^b x_i^u + \frac{1}{2} \left(\beta' J \sqrt{\alpha r} \sum_u x_i^u \right)^2 - \frac{1}{2} n (\beta' J)^2 \alpha r \right) \\
&= \log \prod_i \int Dz \sum_{\mathbf{x}_i} \exp \left(\beta' \sum_{u,b} (H_b + Jm_b) \xi_i^b x_i^u + \beta' J \sqrt{\alpha r} z \sum_u x_i^u - \frac{1}{2} n (\beta' J)^2 \alpha r \right) \\
&= \sum_i \log \int Dz \exp \left(n \log \left(2 \cosh \left(\beta' \sum_b (H_b + Jm_b) \xi_i^b + \beta' J \sqrt{\alpha r} z \right) \right) - \frac{1}{2} n (\beta' J)^2 \alpha r \right) \\
&= \sum_i n \int Dz \log \left(2 \cosh \left(\beta' \sum_b (H_b + Jm_b) \xi_i^b + \beta' J \sqrt{\alpha r} z \right) \right) - \frac{1}{2} n N (\beta' J)^2 \alpha r, \tag{S5.15}
\end{aligned}$$

where in the last step we have used the limit $n \rightarrow 0$.

Overlaps corresponding to non-nominated patterns The order parameter r_{uv} physically represents the covariance of the overlaps corresponding to non-nominated patterns [56, p. 35]. The order parameter is defined as

$$r_{uv} = \frac{1}{\beta' J} \langle z_u z_v \rangle_* = \frac{1}{\beta' J} \frac{\int Dz z_u z_v \exp \left(\frac{1}{2} \sum_{u,v} z_u z_v (\beta' J q_{uv}) \right)}{\int Dz \exp \left(\frac{1}{2} \sum_{u,v} z_u z_v (\beta' J q_{uv}) \right)}. \tag{S5.16}$$

Denoting the quadratic form resulting at the exponential of both integrals Λ_{uv} and integral at the denominator \mathcal{Z} , it follows that $\beta' J r_{uv} = \partial_{\Lambda_{uv}} \log \mathcal{Z}$. The integral \mathcal{Z} corresponds to the determinant of the quadratic form Λ and therefore,

$$\partial_{\Lambda_{uv}} \log \det \Lambda = \text{tr}[\Lambda^{-1} \partial_{\Lambda_{uv}} \Lambda] = \Lambda_{uv}^{-1}, \tag{S5.17}$$

that is, the covariance of z_u, z_v is given by the inverse Λ_{uv}^{-1} . The regularity of Λ_{uv} allows us to compute its inverse via Sherman-Morrison formula,

$$\Lambda_{uv}^{-1} = \frac{1}{1 - \beta' J(1 - q)} \left(1 + \frac{\beta' J q \delta_{uv}}{1 - \beta' J(1 - q) - n \beta' J q} \right), \tag{S5.18}$$

evaluating the limit $n = 0$,

$$\beta' J r_{uv} = \delta_{uv} \frac{1 - \beta' J(1 - 2q)}{(1 - \beta' J(1 - q))^2} + (1 - \delta_{uv}) \frac{\beta' J q}{(1 - \beta' J(1 - q))^2}. \tag{S5.19}$$

Identifying R and r as the respective diagonal and off diagonal parts of r_{uv} , we can determine

$$\mu \xrightarrow{n \rightarrow 0} \frac{1}{2} N \alpha \beta' J (R - q r). \tag{S5.20}$$

This leads to an effective inverse temperature,

$$\beta' = \frac{\beta}{1 + \gamma' \frac{1}{2} \left(\sum_b (2H_b + Jm_b) m_b + \alpha J \left(\frac{1 - \beta' J(1 - q)^2}{(1 - \beta' J(1 - q))^2} - 1 \right) \right)}. \tag{S5.21}$$

Replica symmetric solution We have

$$\begin{aligned}
\frac{1}{n} \log \langle Z^n \rangle &= \frac{N \beta}{\gamma'} \log \left[1 + \gamma' \left(\sum_b \left(H_a m_b + \frac{J}{2} (m_b)^2 \right) + \frac{J}{N} \mu - \frac{J \alpha}{2} \right) \right]_+ \\
&\quad - N \beta' \sum_b (H_b + Jm_b) m_b - \beta' J \mu - \frac{1}{2n} N \alpha \log \det \Lambda - \frac{1}{2} N \alpha (n - 1) (J \beta')^2 r q \\
&\quad + \sum_i \int Dz \log \left(2 \cosh \left(\beta' \sum_b (H_b + Jm_b) \xi_i^b + \beta' J \sqrt{\alpha r} z \right) \right) - \frac{1}{2} N (\beta' J)^2 \alpha r. \tag{S5.22}
\end{aligned}$$

In the limit of $n \rightarrow 0$, we have

$$\begin{aligned} \log \det \mathbf{A} &= \log(1 - \beta' J(1 - q) - \beta' J q n) + (n - 1) \log(1 - \beta' J(1 - q)) \\ &= n \left(\log(1 - \beta' J(1 - q)) - \frac{\beta' J q}{1 - \beta' J(1 - q)} \right) \\ &= n (\log(1 - \beta' J(1 - q)) - \beta' J \sqrt{r q}). \end{aligned} \quad (\text{S5.23})$$

Extremisation with respect to H_a yields:

$$m_a = \frac{1}{N} \sum_i \xi_i^a \int Dz \tanh \left(\beta' \sum_b (H_b + J m_b) \xi_i^b + \beta' J \sqrt{\alpha r} z \right). \quad (\text{S5.24})$$

Similarly, extremisation with respect to r results in

$$\frac{\beta'^2 J^2}{2} N \alpha (1 - q) = N \beta' J \frac{1}{2} \sqrt{\frac{\alpha}{r}} \int Dz \tanh \left(\beta' \sum_b (H_b + J m_b) \xi_i^b + \beta' J \sqrt{\alpha r} z \right) z \quad (\text{S5.25})$$

$$q = \int Dz \tanh^2 \left(\beta' \left(\sum_b (H_b + J m_b) \xi_i^b + J \sqrt{\alpha r} z \right) \right). \quad (\text{S5.26})$$

We can observe that for $\alpha = 0$, we recover previous results in (S3.9). In addition, for $\gamma = 0$, $\beta' = \beta$, and the solution corresponds to the Hopfield model near saturation [56, 60].

Notice that in the limit $J \rightarrow 0$ and $\mathbf{H} = \mathbf{0}$

$$\beta' J^2 \mu = \frac{1}{2} N J \alpha (1 + \beta' J(1 - q^2)) - N \frac{J \alpha}{2}, \quad (\text{S5.27})$$

$$r = q, \quad (\text{S5.28})$$

$$\beta' = \frac{\beta}{1 + \gamma N \beta \frac{1}{2} \alpha \beta' J^2 (1 - q^2)}. \quad (\text{S5.29})$$

For $\alpha = 1$ and $\gamma' = \gamma N \beta \frac{J^2}{2}$ recovering the previous solution in Eqs. (S6.18)-S6.20

3. AT-instability line

This section probes how the deformation of the statistics modifies the boundary below which we may no longer rely on replica symmetry. Following [56] let us then consider small fluctuations η_{uv} around the replica symmetric expressions for q_{uv} and its conjugated pair.

$$q_{uv} \mapsto q_{uv}^{\text{RS}} + \eta_{uv} := \delta_{uv} + q(1 - \delta_{uv}) + \eta_{uv} \quad (\text{S5.30})$$

with $\eta_{uv} = \eta_{vu}$ vanishing diagonal elements and $\sum_u \eta_{uv} = 0$. We are ultimately interested in the free energy difference,

$$\frac{1}{N} \Delta \varphi_\gamma := \frac{1}{N} [\varphi_\gamma(m^{\text{RS}}, q_{uv}, \hat{q}_{uv}) - \varphi_\gamma(m^{\text{RS}}, q_{uv}^{\text{RS}}, \hat{q}_{uv}^{\text{RS}})]. \quad (\text{S5.31})$$

One should be mindful that β'_u may be affected by fluctuations. The inverse temperature β'_u depends on μ , which is itself a function of both q_{uv} and \hat{q}_{uv} . One can anticipate that \hat{q}_{uv} , and thereby β'_u , will be a polynomial in η_{uv} . The coefficients of the perturbative expansion of β'_u are determined by replica-symmetric parameters and hence its index structure followed from the properties of η_{uv} rule out linear contributions. Without loss of generality, we have up to second order,

$$\beta'_u = \beta'_0 + \beta_1 \sum_v \eta_{uv}^2 + \mathcal{O}(\eta^3), \quad (\text{S5.32})$$

for some β_1 to be determined and β'_0 being its RS-value, which only distinguishes between diagonal and off-diagonal components. Solving for β'_0 at (S5.21)

$$\beta'_0 = \frac{2 - \alpha \gamma' + \gamma' m^2 \pm \sqrt{(\alpha \gamma' - \gamma' m^2 - 2)^2 - 8 \beta \alpha \gamma' (q r - R)}}{2 \alpha \gamma' (q r - R)}. \quad (\text{S5.33})$$

To resolve how its conjugate, \hat{q}_{uv} , transforms, we inspect the two-point functions $\langle z_u z_v \rangle_*$ upon small perturbations of the order parameter η_{uv} ,

$$\langle z_u z_v \rangle_* \mapsto \frac{\langle z_a z_b \rangle_* + \frac{1}{2} \sum_{c,d} \langle z_a z_b z_c z_d \rangle_* \Lambda_{cd}}{1 + \frac{1}{2} \sum_{c,d} \langle z_c z_d \rangle_* \Lambda_{cd}} \simeq \langle z_a z_b \rangle_* + \frac{1}{2} \sum_{c,d} \Lambda_{cd} [\langle z_a z_b z_c z_d \rangle_* - \langle z_a z_b \rangle_* \langle z_c z_d \rangle_*] \quad (\text{S5.34})$$

with

$$\Lambda_{cd} = \beta'_0 J \eta_{cd} + \beta_1 J \sum_s (\eta_{cs}^2 + \eta_{ds}^2) [\delta_{cd} + q(1 - \delta_{cd})]. \quad (\text{S5.35})$$

This implies that $\hat{\eta}_{cd}$, defined as the change of the two point function, and thereby \hat{q}_{uv} — conjugate to q_{uv} — carry a dependence of second order in fluctuations parameterised by β_1 .

$$\begin{aligned} \hat{q}_{uv} &= -iN\alpha\sqrt{\beta'_u\beta'_v}J\langle z_u z_v \rangle_* \\ &\rightarrow -iN\alpha J \left(\beta'_0 + \frac{1}{2}\beta_1 \sum_s [\eta_{us}^2 + \eta_{vs}^2] \right) [\langle z_u z_v \rangle_* + \hat{\eta}_{uv}] \\ &= \hat{q}_{uv}^{\text{RS}} - iN\alpha J \left(\beta'_0 \hat{\eta}_{uv} + \frac{1}{2}\beta_1 \sum_s \langle z_u z_v \rangle_* [\eta_{us}^2 + \eta_{vs}^2] \right). \end{aligned} \quad (\text{S5.36})$$

Here β'_1 can be obtained from the expression for β' at (S5.10) noticing the similarity of $\sum_v \beta'_v q_{uv} r_{uv}$ with (S5.44) once perturbed.

$$\begin{aligned} \sum_v q_{uv} \langle z_u z_v \rangle_* &\mapsto \sum_v (q_{uv}^{\text{RS}} + \eta_{uv}) (\langle z_u z_v \rangle_* + \hat{\eta}_{uv}) \\ &= \beta'_0 J (R - rq) + \sum_v (q_{uv}^{\text{RS}} \hat{\eta}_{uv} + \langle z_u z_v \rangle_* \eta_{uv} + \eta_{uv} \hat{\eta}_{uv}) \\ &= \beta'_0 J (R - rq) + \frac{1}{2}\beta_1 \sum_{v,s,c,d} q_{uv}^{\text{RS}} q_{cd}^{\text{RS}} g_{uvcd} (\eta_{cs}^2 + \eta_{ds}^2) + \frac{1}{2}\beta'_0 \sum_{v,c,d} g_{uvcd} \eta_{uv} \eta_{cd}, \end{aligned} \quad (\text{S5.37})$$

where the first term results from its RS-valued part and

$$g_{abcd} = \langle z_a z_b z_c z_d \rangle_* - \langle z_a z_b \rangle_* \langle z_c z_d \rangle_* = \langle z_a z_c \rangle_* \langle z_b z_d \rangle_* + \langle z_a z_d \rangle_* \langle z_b z_c \rangle_* \quad (\text{S5.38})$$

has been adopted for brevity. The four-point function can be reduced via Wick Theorem, to products of two-point functions. Linear terms in fluctuations coupled to RS-terms vanish with the sum as expected. It should be noted that unlike the flat case, $\sum_s \hat{\eta}_{us} = 0$ property no longer holds due to quadratic terms in perturbations.

Let us now evaluate the sums at (S5.37),

$$\begin{aligned} \sum_{v,s,c,d} q_{uv}^{\text{RS}} q_{cd}^{\text{RS}} g_{uvcd} (\eta_{cs}^2 + \eta_{ds}^2) &= \sum_{v,s,c,d} q_{uv}^{\text{RS}} q_{cd}^{\text{RS}} (\langle z_u z_c \rangle_* \langle z_v z_d \rangle_* + \langle z_u z_d \rangle_* \langle z_v z_c \rangle_*) (\eta_{cs}^2 + \eta_{ds}^2) \\ &= (\beta'_0 J)^2 \sum_{v,s,c,d} q_{uv}^{\text{RS}} q_{cd}^{\text{RS}} (r_{uc}^{\text{RS}} r_{vd}^{\text{RS}} + r_{ud}^{\text{RS}} r_{vc}^{\text{RS}}) (\eta_{cs}^2 + \eta_{ds}^2) \end{aligned} \quad (\text{S5.39})$$

from here we break the sums into diagonal and off diagonal contributions

$$\begin{aligned} &= 4(\beta'_0 J)^2 \sum_{v,s,c} q_{uv}^{\text{RS}} r_{uc}^{\text{RS}} r_{vc}^{\text{RS}} \eta_{cs}^2 + 2q(\beta'_0 J)^2 \sum_{v,s,c \neq d} q_{uv}^{\text{RS}} (r_{uc}^{\text{RS}} r_{vd}^{\text{RS}} + r_{ud}^{\text{RS}} r_{vc}^{\text{RS}}) \eta_{cs}^2 \\ &= 4(\beta'_0 J)^2 \sum_{s,c} r_{uc}^{\text{RS}2} \eta_{cs}^2 + 4q(\beta'_0 J)^2 \sum_{v \neq u,s,c} r_{uc}^{\text{RS}} r_{vc}^{\text{RS}} \eta_{cs}^2 + 4q(\beta'_0 J)^2 \sum_{s,c \neq d} r_{ud}^{\text{RS}} r_{uc}^{\text{RS}} \eta_{cs}^2 \\ &\quad + 2q^2(\beta'_0 J)^2 \sum_{s,v \neq u,c \neq d} (r_{uc}^{\text{RS}} r_{vd}^{\text{RS}} + r_{ud}^{\text{RS}} r_{vc}^{\text{RS}}) \eta_{cs}^2. \end{aligned} \quad (\text{S5.40})$$

Evaluation of $r_{ud}^{\text{RS}} = R\delta_{ud} + r(1 - \delta_{ud})$ yields a polynomial we will call for the moment $f(q, \beta'_0, r, R)$, and so the expression may be succinctly written as $f(q, \beta'_0, r, R) \sum_s \eta_{us}^2$. More importantly,

$$\begin{aligned} \sum_{v,c,d} g_{uvcd} \eta_{uv} \eta_{cd} &= (\beta'_0 J)^2 \sum_{v,c,d} (r_{uc}^{\text{RS}} r_{vd}^{\text{RS}} + r_{ud}^{\text{RS}} r_{vc}^{\text{RS}}) \eta_{uv} \eta_{cd} \\ &= (\beta'_0 J)^2 \sum_{v \neq u, c \neq d} (r_{uc}^{\text{RS}} r_{vd}^{\text{RS}} + r_{ud}^{\text{RS}} r_{vc}^{\text{RS}}) \eta_{uv} \eta_{cd} \\ &= 2(\beta'_0 J)^2 \sum_{v \neq u, c \neq d} r_{uc}^{\text{RS}} r_{vd}^{\text{RS}} \eta_{uv} \eta_{cd} = 2(\beta'_0 J)^2 \sum_{c \neq d} r_{uc}^{\text{RS}} \left(\sum_{v \neq u} r_{vd}^{\text{RS}} \eta_{uv} \right) \eta_{cd} = 0. \end{aligned} \quad (\text{S5.41})$$

Now we can solve for β_1 , expanding the self-consistent equation,

$$\begin{aligned} \beta'_0 + \beta_1 \sum_s \eta_{vs}^2 &\simeq \beta'_0 \left(1 - \frac{1}{4\Gamma} \gamma' \alpha J \left(\beta_1 \sum_{v,s,c,d} q_{uv}^{\text{RS}} q_{cd}^{\text{RS}} g_{uvcd} (\eta_{cs}^2 + \eta_{ds}^2) + \beta'_0 \sum_{v,c,d} g_{uvcd} \eta_{uv} \eta_{cd} \right) \right) \\ \beta_1 \sum_s \eta_{vs}^2 &\simeq -\frac{1}{4\Gamma} \gamma' \alpha J \beta_1 f(q, \beta'_0, r, R) \sum_s \eta_{us}^2, \end{aligned} \quad (\text{S5.42})$$

where Γ is defined as denominator of the expression for β' at (24),

$$\Gamma := 1 + \frac{1}{2} \gamma' (Jm^2 + \alpha J(\beta'(R - qr) - 1)) \quad (\text{S5.43})$$

seeming to imply that β' does not seem to be altered at second order of perturbations and perhaps the effects are only seen at higher order. This greatly simplifies the analysis onwards; \hat{q}_{uv} and $\hat{\eta}_{uv}$ are now first order in η_{uv} , the latter reduced to $\hat{\eta}_{uv} = \beta_0'^2 (R - r)^2 \eta_{uv}$. The same expression for $\gamma = 0$ up to a scaled inverse temperature, are recovered. Let us focus on the free energy difference,

$$\begin{aligned} \frac{1}{N} \Delta \varphi_\gamma &\ni \frac{1}{2N} \sum_{u,v} (i \hat{q}_{uv} q_{uv} - i \hat{q}_{uv}^{\text{RS}} q_{uv}^{\text{RS}}) = \frac{i}{2N} \text{Tr} [\hat{q}_{uv}^{\text{RS}} \eta_{uv}] + \frac{1}{2} \alpha (\beta' J)^2 \text{Tr} [\hat{\eta}_{uv} \hat{q}_{uv}^{\text{RS}} + \hat{\eta}_{uv} \eta_{uv}] \\ &= \frac{1}{2} \alpha (\beta' J)^2 \text{Tr} [\hat{\eta}_{uv} \eta_{uv}]. \end{aligned} \quad (\text{S5.44})$$

the trace is understood over replica indices. Notice that despite the seemingly different overall coefficient and sign [56], this is just an artifact of the convention on the introduction of the deltas, these expressions are equivalent. The diagonal terms included to make up the trace vanish as constants at the free energy difference.

The determinants transform as,

$$\frac{1}{N} \Delta \varphi_\gamma \ni \log \frac{\det[1 - \beta'(q_{uv}^{\text{RS}} + \eta_{uv})]}{\det[1 - \beta' q_{uv}^{\text{RS}}]} = -\frac{1}{2} \frac{\beta_0'^2}{[1 - \beta_0'(1 - q)]^2} \text{Tr} \boldsymbol{\eta}^2 + \mathcal{O}(\boldsymbol{\eta}^3). \quad (\text{S5.45})$$

There is a contribution from the $L(x_i)$ -function and the logarithm that results from the deformation. First the L -term contribution

$$\frac{1}{N} \Delta \varphi_\gamma \ni \log \frac{\sum_{\mathbf{x}} \exp L(m^{\text{RS}}, q_{uv}, \hat{q}_{uv}, x_i)}{\sum_{\mathbf{x}} \exp L(m^{\text{RS}}, q_{uv}^{\text{RS}}, \hat{q}_{uv}^{\text{RS}}, x_i)}, \quad (\text{S5.46})$$

which basically amounts to, after expansion,

$$\begin{aligned} \log \sum_{\mathbf{x}} \exp L(m^{\text{RS}}, q_{uv}, \hat{q}_{uv}, x_i) &\simeq \log \prod_i \sum_{\mathbf{x}_i} \exp \Lambda^{\text{RS}}(x_i) \left[1 + \alpha J^2 \sum_{u,v} x_i^u \hat{\eta}_{uv} x_i^v \sum_{u,v} \beta'_{0u} \eta_{uv} \beta'_{1v} \right. \\ &\quad \left. + \frac{1}{2} \alpha J^2 \beta_0'^2 \sum_{u,v} x_i^u \hat{\eta}_{uv} x_i^v + \frac{1}{8} \alpha^2 (\beta'_0 J)^4 \sum_{u,v} (x_i^u \hat{\eta}_{uv} x_i^v)^2 \right]. \end{aligned} \quad (\text{S5.47})$$

However, as we concluded previously β'_u does not have second order term.

$$= \log \prod_i \sum_{\mathbf{x}_i} \exp \Lambda^{\text{RS}}(x_i) \left[1 + \frac{1}{2} \alpha (\beta'_0 J)^2 \sum_{u,v} x_i^u \hat{\eta}_{uv} x_i^v + \frac{1}{8} \alpha^2 (\beta'_0 J)^4 \sum_{u,v} (x_i^u \hat{\eta}_{uv} x_i^v)^2 \right], \quad (\text{S5.48})$$

where $\Lambda^{\text{RS}}(x_i)$ has been defined as the argument of the exponential at (S5.15). Once again the trace can be recovered at the fluctuation terms can be recovered noticing that $\eta_{uu} = 0$. The denominator eventually cancels off the contributions from $\Lambda^{\text{RS}}(x_i)$, and we are left with the part from the squared brackets. The first term can be recognised as the average defined at the saddle-node solution for q_{ab} (S5.10). Finally, the logarithm that amounts from the deformation of the statistics and μ ,

$$\frac{1}{N}\Delta\varphi_\gamma \ni \frac{\beta}{\gamma'} \log\left(\frac{\beta'_{\text{RS}}}{\beta'}\right) - \beta' J\Delta\mu = 0 \quad (\text{S5.49})$$

are up to second order in perturbations, invariant, and hence do not contribute to the free energy difference. Following the derivation of $\Delta\varphi_\gamma$ for $\gamma \rightarrow 0$ at [56], we may determine,

$$\begin{aligned} \frac{1}{N}\Delta\varphi_\gamma = \frac{1}{\beta'_0 n} & \left(-\frac{1}{4} \frac{\alpha\beta_0'^2}{[1 - \beta'_0(1 - q)]_+^2} \text{Tr} \boldsymbol{\eta}^2 + \frac{1}{2} \alpha\beta_0'^4 (R - r)^2 \text{Tr} \boldsymbol{\eta}^2 \right. \\ & \left. - \frac{1}{8} \alpha^2 \beta_0'^8 (R - r)^4 \sum_{a,b,c,d} \eta_{ab} \eta_{cd} G_{abcd} \right), \end{aligned} \quad (\text{S5.50})$$

where

$$\begin{aligned} G_{abcd} = & \delta_{ac}\delta_{bd} + \delta_{ad}\delta_{bc} + G_4(1 - \delta_{ac})(1 - \delta_{bd})(1 - \delta_{ad})(1 - \delta_{bc}) \\ & + G_2(\delta_{ac}(1 - \delta_{bd}) + \delta_{bd}(1 - \delta_{ac}) + \delta_{ad}(1 - \delta_{bc}) + \delta_{bc}(1 - \delta_{ad})), \end{aligned} \quad (\text{S5.51})$$

leading to a condition

$$(1 + \beta'_0(1 - q))^2 > \alpha\beta_0'^2 \frac{1}{N} \sum_i \xi_i^a \int Dz \cosh^{-4} \beta'_0 \left(\sum_b (H_b + Jm_b) \xi_i^b + J\sqrt{\alpha r} z \right) \quad (\text{S5.52})$$

equivalent to that of the flat model (see [56], equation (121)) with a re-scaled inverse temperature.

Supplementary Note 6: Curved Sherrington-Kirkpatrick model

We start with a simple case in which the system is encoding one pattern on a background of zero-average Gaussian weights. This can be represented by $J_{ij} = J_0/N\xi_i\xi_j + J/\sqrt{N}z_{ij}$, with z_{ij} random coupling values distributed as $\mathcal{N}(0, 1)$. Assuming the content of the $[\]_+$ operator is positive, we want to compute the configurational average

$$\begin{aligned}\langle\langle\varphi_\gamma\rangle\rangle &= \int d\mathbf{z} p(\mathbf{z}) \log \sum_{\mathbf{x}} \left(1 + \gamma\beta \left(\frac{J_0}{N} \sum_{i<j} x_i \xi_i \xi_j x_j + \frac{J}{\sqrt{N}} \sum_{i<j} z_{ij} x_i x_j \right) \right)^{1/\gamma} \\ &= \int d\mathbf{z} p(\mathbf{z}) \log \sum_{\mathbf{x}} \left(1 + \gamma\beta \left(\frac{NJ_0}{2} \left(\frac{1}{N} \sum_i x_i \xi_i \right)^2 - \frac{J_0}{2} + \frac{J}{\sqrt{N}} \sum_{i<j} z_{ij} x_i x_j \right) \right)^{1/\gamma}.\end{aligned}\quad (\text{S6.1})$$

Defining $\varphi_\gamma = \log Z$, we can apply the replica method

$$\langle\langle\varphi_\gamma\rangle\rangle = \langle\langle\log Z\rangle\rangle = \lim_{n \rightarrow 0} \frac{1}{n} (\langle\langle Z^n \rangle\rangle - 1) \quad \text{or, equivalently,} \quad \langle\langle\log Z\rangle\rangle = \lim_{n \rightarrow 0} \frac{1}{n} \log \langle\langle Z^n \rangle\rangle, \quad (\text{S6.2})$$

with

$$\langle\langle Z^n \rangle\rangle = \int d\mathbf{z} p(\mathbf{z}) \sum_{\mathbf{x}} \exp \left(\sum_u \frac{1}{\gamma} \log \left[1 + \gamma\beta \left(\frac{NJ_0}{2} \left(\frac{1}{N} \sum_i x_i^u \xi_i \right)^2 - \frac{J_0}{2} + \frac{J}{\sqrt{N}} \sum_{i<j} z_{ij} x_i^u x_j^u \right) \right] \right) \quad (\text{S6.3})$$

$$\begin{aligned}&= \frac{1}{(2\pi)^{2n}} \int d\mathbf{z} p(\mathbf{z}) \sum_{\mathbf{x}} d\mathbf{m} d\hat{\mathbf{m}} d\boldsymbol{\mu} d\hat{\boldsymbol{\mu}} \exp \left(\frac{1}{\gamma} \sum_u \log \left(1 + \gamma\beta \left(\frac{NJ_0}{2} m_u^2 - \frac{J_0}{2} + J\mu_u \right) \right) \right. \\ &\quad \left. - \sum_u i\hat{m}_u \left(m_u - \frac{1}{N} \sum_i \xi_i x_i^u \right) - \sum_u i\hat{\mu}_u \left(\mu_u - \frac{1}{\sqrt{N}} \sum_{i<j} z_{ij} x_i^u x_j^u \right) \right).\end{aligned}\quad (\text{S6.4})$$

Recalling that the \mathbf{z} couplings are distributed by a centred Gaussian $\mathcal{N}(0, 1)$, we can carry out explicit integration of z_{ij} . Noting that $\int \mathcal{D}\mathbf{z} e^{\lambda\mathbf{z}} = e^{\lambda^2/2}$, the above may be rewritten as,

$$\begin{aligned}&= \frac{1}{(2\pi)^{2n}} \int d\mathbf{m} d\hat{\mathbf{m}} d\boldsymbol{\mu} d\hat{\boldsymbol{\mu}} \sum_{\mathbf{x}} \exp \left(\frac{1}{\gamma} \sum_u \log \left(1 + \gamma\beta \left(\frac{NJ_0}{2} m_u^2 - \frac{J_0}{2} + J\mu_u \right) \right) \right. \\ &\quad \left. - \sum_u i\hat{m}_u \left(m_u - \frac{1}{N} \sum_i \xi_i x_i^u \right) - \sum_u i\hat{\mu}_u \mu_u + \frac{1}{4N} \sum_{i \neq j} \left(\sum_u i\hat{\mu}_u x_i^u x_j^u \right)^2 \right).\end{aligned}\quad (\text{S6.5})$$

The last term at the exponential can be expressed as,

$$N \frac{1}{2} \sum_{u < v} i\hat{\mu}_u i\hat{\mu}_v \left(\left(\frac{1}{N} \sum_i x_i^u x_i^v \right)^2 - \frac{1}{N} \right) - N \frac{1}{4} \sum_u (i\hat{\mu}_u)^2 \left(1 - \frac{1}{N} \right). \quad (\text{S6.6})$$

Furthermore, introducing conjugate pair fields for the average of $x_i^u x_i^v$, $\{\mathbf{q}, \hat{\mathbf{q}}\}$ we have,

$$\begin{aligned}&(2\pi)^{-2n-n(n-1)} \int d\mathbf{m} d\hat{\mathbf{m}} d\boldsymbol{\mu} d\hat{\boldsymbol{\mu}} d\mathbf{q} d\hat{\mathbf{q}} \\ &\sum_{\mathbf{x}} \exp \left(\frac{1}{\gamma} \sum_u \log \left(1 + \gamma\beta \left(\frac{NJ_0}{2} m_u^2 - \frac{J_0}{2} + J\mu_u \right) \right) - N \frac{1}{4} \sum_u (i\hat{\mu}_u)^2 \left(1 - \frac{1}{N} \right) - \sum_u i\hat{\mu}_u \mu_u \right. \\ &\quad \left. - \sum_u i\hat{m}_u \left(m_u - \frac{1}{N} \sum_i \xi_i x_i^u \right) - \sum_{u < v} i\hat{q}_{uv} \left(q_{uv} - \frac{1}{N} \sum_i x_i^u x_i^v \right) + N \frac{1}{2} \sum_{u < v} i\hat{\mu}_u i\hat{\mu}_v \left(q_{uv}^2 - \frac{1}{N} \right) \right).\end{aligned}\quad (\text{S6.7})$$

Now we can evaluate the integrals by steepest descent

$$\begin{aligned}
&= \exp \left\{ \frac{1}{\gamma} \sum_u \log \left(1 + \gamma \beta \left(\frac{NJ_0}{2} m_u^2 - \frac{J_0}{2} + J\mu_u \right) \right) - N \frac{1}{4} \sum_u (\hat{\mu}_u)^2 \left(1 - \frac{1}{N} \right) \right. \\
&\quad \left. - \sum_u i\hat{m}_u m_u - \sum_u i\hat{\mu}_u \mu_u - \sum_{u < v} i\hat{q}_{uv} q_{uv} + \frac{1}{2} N \sum_{u < v} i\hat{\mu}_u i\hat{\mu}_v \left(q_{uv}^2 - \frac{1}{N} \right) + \log \sum_{\mathbf{x}} \exp L \right\}. \quad (\text{S6.8})
\end{aligned}$$

The overall 2π factor has been left out as we are ultimately concerned with $n \rightarrow 0$. With L corresponding to the x_i -dependant part in the argument of the exponential (S5.9). Here, (S6.8) is to be understood at the saddle-node solution, which ignoring the $\mathcal{O}(\frac{1}{N})$ terms corresponds to,

$$i\hat{m}_u = \beta'_u N J_0 m_u, \quad (\text{S6.9a})$$

$$i\hat{\mu}_u = \beta'_u J, \quad (\text{S6.9b})$$

$$m_u = \langle x_i^u \rangle, \quad (\text{S6.9c})$$

$$q_{uv} = \langle x_i^u x_i^v \rangle, \quad (\text{S6.9d})$$

$$\hat{q}_{uv} = N i\hat{\mu}_u i\hat{\mu}_v q_{uv} = (\beta'_u J)^2 q_{uv}, \quad (\text{S6.9e})$$

$$\mu_u = N \frac{1}{2} \sum_v i\hat{\mu}_v q_{uv}^2 = N J \frac{1}{2} \sum_v \beta'_v q_{uv}^2, \quad (\text{S6.9f})$$

$$\beta'_u = \frac{\beta}{1 + \gamma \beta (N \frac{1}{2} J_0 m_u^2 + \mu_u)} = \frac{\beta}{1 + \gamma \beta N \frac{1}{2} (J_0 m_u^2 + J^2 \sum_v \beta'_v q_{uv}^2)}. \quad (\text{S6.9g})$$

Assuming $q_{uu} = 1$, we can rewrite (S6.8) by evaluating at (S6.9). As we are contemplating the $n \rightarrow 0$ limit, N is taken large but kept at fixed value, resulting in

$$\begin{aligned}
\langle\langle Z^n \rangle\rangle &= 1 + \frac{1}{\gamma} \sum_u \log \left(1 + \gamma \beta \left(\frac{NJ_0}{2} m_u^2 - \frac{J_0}{2} + N J^2 \frac{1}{2} \sum_v \beta'_v q_{uv}^2 \right) \right) \\
&\quad - \sum_u \beta'_u N J_0 m_u^2 - N \frac{3}{4} \sum_{u,v} \beta'_u \beta'_v J^2 q_{uv}^2 + \log \sum_{\mathbf{x}} \exp L. \quad (\text{S6.10})
\end{aligned}$$

In the limit $\gamma \rightarrow 0$, we recover the replica free-energy of the SK model

$$\langle\langle \varphi_\gamma \rangle\rangle = -\beta N \frac{J_0}{2n} \sum_u m_u^2 - N \frac{\beta^2 J^2}{4n} \sum_{u,v} q_{uv}^2 + \log \sum_{\mathbf{x}} \exp L. \quad (\text{S6.11})$$

1. Replica symmetry

The assumption of replica symmetry implies homogeneous couplings among replicas $q_{uv} = \delta_{uv} + q(1 - \delta_{uv})$. Also we will consider $m_u = m$ for the mean field,

$$\begin{aligned}
\langle\langle \varphi_\gamma \rangle\rangle &= \frac{1}{\gamma} \log \left[1 + \gamma \beta \left(\frac{NJ_0}{2} m^2 - \frac{J_0}{2} + N J^2 \frac{1}{2} \beta' (1 - q^2) \right) \right]_+ \\
&\quad - \beta' N J_0 m^2 - N \frac{3}{4} \beta'^2 J^2 (1 - q^2) + \frac{1}{n} \log \sum_{\mathbf{x}} \exp L \quad (\text{S6.12})
\end{aligned}$$

with L carrying the \mathbf{x} dependence. We can further simplify evaluating the sum,

$$\begin{aligned}
\log \sum_{\mathbf{x}} \exp L &= \log \sum_{\mathbf{x}} \exp \left(n\beta' J_0 m \sum_i \xi_i x_i^u + \sum_i (\beta' J)^2 q \sum_i \sum_{u < v} x_i^u x_i^v \right) \\
&= \log \prod_i \sum_{\mathbf{x}_i} \exp \left(\sum_u \beta'_u J_0 m \xi_i x_i^u + \frac{1}{2} \left(\beta' J \sqrt{q} \sum_u x_i^u \right)^2 - \frac{1}{2} n (\beta' J)^2 q \right) \\
&= \log \prod_i \int Dz \sum_{\mathbf{x}_i} \exp \left(\sum_u \beta'_u J_0 m x_i^u + \beta' J \sqrt{q} z \sum_u x_i^u - \frac{1}{2} n (\beta' J)^2 q \right) \\
&= N \log \int Dz \exp (n \log (2 \cosh (\beta' J_0 m + \beta' J \sqrt{q} z))) - \frac{1}{2} n N (\beta' J)^2 q \\
&\approx N n \int Dz \log (2 \cosh (\beta' J_0 m + \beta' J \sqrt{q} z)) - \frac{1}{2} n N (\beta' J)^2 q
\end{aligned} \tag{S6.13}$$

replacing values,

$$\frac{1}{N} \langle N \varphi \rangle = \frac{1}{\gamma} \log \left(1 + \gamma \beta \left(\frac{J_0}{2} m^2 + J^2 \frac{1}{2} \beta' (1 - q^2) \right) \right) \tag{S6.14}$$

$$- \beta' J_0 m^2 - \frac{3}{4} \beta'^2 J^2 (1 - q^2) + \int Dz \log (2 \cosh (\beta' J_0 m + \beta' J \sqrt{q} z)) - \frac{1}{2} (\beta' J)^2 q. \tag{S6.15}$$

Extremisation with respect to m and q yields:

$$\beta' J_0 m = \beta' J_0 \int Dz \tanh (\beta' J_0 m + \beta' J \sqrt{q} z) \tag{S6.16}$$

$$\frac{\beta'^2 J^2}{2} (1 - q) = \beta' J \frac{1}{2\sqrt{q}} \int Dz \tanh (\beta' J_0 m + \beta' J \sqrt{q} z) z, \tag{S6.17}$$

leading to the solution, for $\gamma' = \gamma/(N\beta)$:

$$m = \int Dz \tanh (\beta' (J_0 m + J \sqrt{q} z)), \tag{S6.18}$$

$$q = \int Dz \tanh^2 (\beta' (J_0 m + J \sqrt{q} z)), \tag{S6.19}$$

$$\beta' = \frac{\beta}{1 + \gamma' (\frac{1}{2} J_0 m^2 + \frac{1}{2} \beta' J^2 (1 - q^2))}. \tag{S6.20}$$

a. Critical point

The solution for $J_0 = 0, J = 1$ at $\gamma' = 0$ has the form

$$q = \int Dz \tanh^2 (\beta \sqrt{q} z). \tag{S6.21}$$

Using a change of variables $\rho = \sqrt{q}$ we can expand around $\rho \rightarrow 0$

$$\begin{aligned}
q &= \int Dz \tanh^2 (\beta' \rho z) = \beta'^2 \rho^2 - 2\beta'^4 \rho^4 + \mathcal{O}(\rho^6) \\
&= \beta'^2 q - 2\beta'^4 q^2 + \mathcal{O}(q^3).
\end{aligned} \tag{S6.22}$$

With a trivial solution $q = 0$, and a solution

$$q = \frac{1}{2\beta^4} (\beta^2 - 1) \tag{S6.23}$$

when $\beta' > 1$.

With a slope of

$$\frac{\partial q}{\partial \beta} = \frac{1}{\beta^5}(2 - \beta^2), \quad (\text{S6.24})$$

which is equal to 1 at the critical point.

For $\gamma' \neq 0$, we can recover the critical solution by a change of variables $\beta \rightarrow \beta'$. For $m = 0$, the solution of (S6.19) for an arbitrary β' is the same as the solution of (S6.21) for $\beta = \beta'$. For each pair of β', q solving (S6.19), we can recover the corresponding inverse temperature from (S6.20) as $\beta = \beta'(1 + \frac{1}{2}\beta'J^2(1 - q^2))$.

At the critical point $\beta' = 1$ and $q = 0$, then we have

$$\beta' + \beta'^2\gamma'\frac{1}{2} = \beta, \quad (\text{S6.25})$$

thus the critical point will be located at

$$\beta_c = 1 + \frac{1}{2}\gamma'. \quad (\text{S6.26})$$

The derivative of β' yields

$$\frac{d\beta'}{d\beta}(1 + \beta'\gamma') = 1 \quad (\text{S6.27})$$

$$\frac{d\beta'}{d\beta} = \frac{1}{1 + \beta'\gamma'}. \quad (\text{S6.28})$$

Resulting then in a slope of

$$\frac{\partial q}{\partial \beta} = \frac{\partial q}{\partial \beta'} \frac{\partial \beta'}{\partial \beta} = \frac{1}{\beta'^5} \frac{2 - \beta'^2}{1 + \beta'\gamma'}, \quad (\text{S6.29})$$

which, for $\beta' = 1$ diverges at $\gamma' = 1$, resulting in a second-order phase transition.